

HYDRAULIC CONDUCTIVITY'S IMPACT ON RISE OF EXCESS PORE-WATER
PRESSURE DURING SEISMIC-INDUCED LIQUEFACTION

by

Holly Gunderson



A thesis

submitted in partial fulfillment

of the requirements for the degree of
Master of Science in Civil Engineering

Boise State University

August 2023

© 2023

Holly Gunderson

ALL RIGHTS RESERVED

BOISE STATE UNIVERSITY GRADUATE COLLEGE

DEFENSE COMMITTEE AND FINAL READING APPROVALS

of the thesis submitted by

Holly Elizabeth Gunderson

Thesis Title: Hydraulic Conductivity's Impact on Rise of Excess
Pore-Water Pressure during Seismic-induced Liquefaction

Date of Final Oral Examination: 13 June 2023

The following individuals read and discussed the thesis submitted by student Holly Elizabeth Gunderson, and they evaluated the student's presentation and response to questions during the final oral examination. They found that the student passed the final oral examination.

Arvin Farid, P.E., Ph.D. Chair, Supervisory Committee Bhaskar

Chittoori, P.E., Ph.D. Member, Supervisory Committee Qifei

Niu, Ph.D. Member, Supervisory Committee

The final reading approval of the thesis was granted by Arvin Farid, P.E., Ph.D.,
Chair of the Supervisory Committee. The thesis was approved by the Graduate College.

DEDICATION

This research is dedicated to my parents, Rebecca and Daniel Gunderson, my three sisters, Amanda, Alison, and Katy, and all my friends for their tireless support and love throughout this journey. I'd also like to dedicate this to my grandparents, Richard, and Hazel Matthews, for inspiring me to always follow my dreams and to never stop learning

ACKNOWLEDGMENTS

I would like to express my gratitude to my advisor, Dr. Arvin Farid, for his constant support, guidance, and motivation during my journey through graduate school. I would like to thank Dr. Bhaskar Chittoori and Dr. Qifei Niu for generously participating in my committee. Special thanks to Griff Allen, Charles Burnell, and Phil Robertson for their contribution in designing, constructing, and maintaining the customized box utilized in this project. Their efforts were instrumental in ensuring the successful execution of this project. And a final thanks to Alyssa Churchfield for helping me prepare soil samples.

ABSTRACT

Liquefaction is a geohazard causing loss of lives and infrastructure around the world. During earthquakes the shaking of the ground may cause a loss of soil strength that results in the settlement of buildings, landslides, failure of earth dams, amongst other hazards (Liquefaction of Soils During Earthquakes, 1985). Liquefaction is the result of a sudden increase in the pore- water pressure (PWP)— referred to as excess pore-water pressure (EPWP)— in loose, saturated, noncohesive, fine soils during seismic shaking. Due to the small pores and low hydraulic conductivity of these soils, the shaking-induced EPWP has less time to dissipate, leading to the loss of the effective stress and, in turn, frictional shear strength of the soil (referred to as liquefaction). If a soil's hydraulic conductivity could be increased during seismic shaking, ample time would be afforded for EPWP dissipation. A potential theory, introduced by our research team, is that electromagnetic (EM) waves can increase granular soils' hydraulic conductivity. This increase can potentially lead to liquefaction mitigation.

This research investigates the relationship between hydraulic conductivity and EPWP buildup, evaluates EM waves' impact on the EPWP buildup by modifying hydraulic conductivity, and evaluates the potential of EM-induced liquefaction mitigation.

Hydraulic conductivity measurement was performed on natural sand. A series of tests were conducted within a customized box featuring two inner flexible walls (to enable shear deformation) constructed of Plexiglas. Constant-head, ASTM-D2434 (2010)

tests were performed to measure the hydraulic conductivity of natural sand samples. All sides of the box containing samples were covered with transparent electrically conductive films, and the medium was excited with electromagnetic waves of various frequencies and power levels— using a radio frequency (RF) signal generator and RF amplifier—to alter the hydraulic conductivity of the soil.

To simulate an earthquake, a shaking table, measuring 11.76 cm × 152.4 cm × 3.81 cm (44 in. × 60 in. × 1.5 in.) excited by a programmable signal generator, was utilized. Additionally, a pore-pressure transducer measured the PWP during experiments. Various experiments were used to evaluate the frequencies and acceleration at which liquefaction occurred. The process was repeated, maintaining consistent seismic frequency and acceleration, to induce excitation of the medium and elevate hydraulic conductivity. Concurrently, the rise of EPWP, the occurrence of liquefaction, and the extent of soil settlement were measured and monitored

TABLE OF CONTENTS

DEDICATION	iv
ACKNOWLEDGMENTS	v
ABSTRACT	vi
LIST OF TABLES	x
LIST OF FIGURES	xi
LIST OF ABBREVIATIONS	xiv
CHAPTER ONE: INTRODUCTION	1
CHAPTER TWO: ELECTROMAGNETIC WAVES IMPACT ON HYDRAULIC CONDUCTIVITY OF GRANULAR SOILS	4
Abstract	4
Theoretical Background	7
Hydraulic Conductivity	7
Liquefaction	9
Electromagnetic Waves	10
Methodology	11
RF Wave Setup	13
Electric Field Mapping	16
3D Numerical Forward Model of Seepage for Hydraulic Conductivity Tests	18
Results and Discussion	21

Electric-Field Measurement and Validation of Numerical Simulation	21
Hydraulic Conductivity Tests	24
Seepage Flow Numerical Simulation	33
Conclusion and Recommendations	39
References	41
CHAPTER THREE: HYDRAULIC CONDUCTIVITY’S IMPACT ON RISE OF EXCESS PORE- WATER PRESSURE DURING SEISMIC-INDUCED LIQUEFACTION	44
Abstract	44
Introduction	45
Background	46
Liquefaction	51
Electromagnetic Waves	55
Methodology	55
Experiment Setup and Testing Procedures	55
Experiment I – Simulated Hydraulic Conductivity Tests using EM Waves	56
Experimental II – Potential Liquefaction Mitigation Tests	59
Experiment I - Hydraulic Conductivity and impact of RF Waves	61
Experiment II – Potential Liquefaction Mitigation	66
Conclusion and Recommendations	75
References	77
Chapter Four: Conclusions	80
Conclusions and Recommendations	80
Future Research	81

LIST OF TABLES

Table 1	Ranges of Intrinsic Permeability and Hydraulic Conductivity for Unconsolidated Sediments (Fetter, 2001)	8
Table 2	Properties of Glass Beads (Najafi, 2014)	14
Table 3	Hydraulic Conductivity Measurements of the Glass-Bead Sample at a Frequency of 726 MHz and Various RF-Power Levels	27
Table 4	Hydraulic Conductivity Measurements of the Natural Sand Sample at a Frequency of 726 MHz and Various RF-Power Levels	30
Table 5	Experimentally Measured and Numerically Computed Flow Discharge in the Natural Sand Sample at Various RF-Power Levels	35
Table 6	Summary of Results from Constant Head Hydraulic Conductivity Tests	66
Table 7	Summary of results from seismic-induced shaking experiments	71
Table 8	Percentage of an Error on Pore-Water Pressure From EM Waves	73
Table 9	Summary of Results From Viscosity of Water Due to Temperature Change During Stimulation at 40 Watts	75

LIST OF FIGURES

- Figure 1 Shows the Schematic of the Setup Used for Launching RF Into the DUT.
14
- Figure 2 Schematic of Customized, Rigid-Wall Cylindrical Permeameter Designed to Conduct RF-Stimulated Hydraulic Conductivity Tests on Sand
16
- Figure 3 Schematic of RF-Stimulation Setup 16
- Figure 4 Schematic Top View of Customized Permeameter with Location of Depth Slices for Hydraulic Conductivity Tests 17
- Figure 5 Schematic of (a) Top View of Discretized Rectangular-Cubical Domain with Circular Cross Section; (b) 3D View of Rectangular-Cubical Domain and Cylindrical Region Within Sample 18
- Figure 6 Schematic of the Location of Depth of Vertical Slices in 3D21
- Figure 7 Electric field: Experimentally Measured (Right) and Numerically Simulated Using COMSOL Multiphysics (left) at 498 MHz Within Glass-bead Sample: A) Depth Slice 1; and B) Depth Slice 2; C) Depth Slice 1; and D) DepthSlice 2 23
- Figure 8 Measured Unstimulated Hydraulic Conductivity in the Glass-bead Sample
24
- Figure 9 Measured RF-Stimulated Hydraulic Conductivity of Glass-bead Sample at a Frequency of 726 MHz and RF-power Levels of: A) 10 Watts; B) 25 Watts; and C) 40 Watts 25
- Figure 10 Measured Unstimulated Hydraulic Conductivity of a Natural Sand Sample 28
- Figure 11 Measured RF-stimulated Hydraulic Conductivity of Natural Sand Samples at a Frequency of 726 MHz and RF-power Levels of: A) 10 Watts; B) 25 Watts; and C) 40 Watts 29

Figure 12	Electric field, Experimentally Measured (right) and Numerically Simulated Using COMSOL Multiphysics (left) Within glass-bead sample on: A) Depth Slice 1, frequency = 710 MHz; B) Depth Slice 2, Frequency = 710 MHz; C) Depth Slice 1, Frequency = 726 MHz	32
Figure 13	Contour/Color Maps of Hydraulic Head (m) for Natural Sand	33
Figure 14	RF-Stimulation Flow Rate v. RF-Power for Natural Sand Specimen	35
Figure 15	Contour/Color Maps of Hydraulic Head (m) on: A) Depth Slices 1 and 15, and Depth Slices 2 and 14, at a Frequency of 726 MHz and RF-Power Level of 25 Watts; B) Depth Slices 3 and 13, and Depth Slices 4 and 12, at a Frequency of 726 MHz and RF-Power 25 Watts; C/ Depth Slices 5 and 11, and Depth Slices 6 and 10, at a Frequency of 726 MHz and RF-Power Level of 25 Watts; D) Depth Slices 7 and 9, and Depth Slice 8, at a Frequency of 726 MHz and RF-Power Level of 25 Watts for Natural Sand Specimen	37
Figure 16	Contour/Color Map of Normalized Difference Between RF-Stimulated Hydraulic Conductivity Computed and Unstimulated Hydraulic Conductivity for Natural Sand Specimen Along the Vertical (Z) Direction on Slice 7	38
Figure 17	Contour/Color Map of Normalized Power Density for Natural Sand Specimen Along the Vertical (Z) Direction on Slice 7	38
Figure 18	Schematic of Flow Path During Liquefaction (Ueng et al., 2017)	51
Figure 19	Schematic of RF Launching Setup	57
Figure 20	Schematic of Customized Box	58
Figure 21	Schematic of Seismic Shaking Launch Setup	59
Figure 22	Constant Head Hydraulic Conductivity Test Performed at 0 Watts	62
Figure 23	Constant Head Hydraulic Conductivity Test Performed at 10 Watts	62
Figure 24	Constant Head Hydraulic Conductivity Test Performed at 20 Watts	64
Figure 25	Constant Head Hydraulic Conductivity Test Performed at 40 Watts	64
Figure 26	Pore-water Pressure During Seismic-induced Shaking at 0 Watts	68
Figure 27	Pore-water Pressure During Seismic-induced Shaking at 10 Watts	68

Figure 28	Pore-water Pressure During Seismic-induced Shaking at 20 Watts	69
Figure 29	Pore-water Pressure During Seismic-induced Shaking at 40 Watts	69
Figure 30	Viscosity Variations Due to Temperature Change During Stimulation at 40 Watts	74

LIST OF ABBREVIATIONS

EPWP	Excess Pore-water Pressure
PWP	Pore-water Pressure
EM	Electromagnetic
RF	Radio Frequency
VNA	Vector Network Analyzer
DUT	Device Under Testing
DAQ	Data Acquisition Device

CHAPTER ONE: INTRODUCTION

Liquefaction, a geohazard of significant concern, has been observed as a destructive force, leading to the loss of lives and infrastructure on a global scale. This phenomenon has been observed in numerous earthquakes such as in 2011 Christchurch, New Zealand (Curbinovski, 2013), 2018 Palu, Sulawesi Island, Indonesia (Tehusijarana, 2018), and in 1985 Mexico City, Mexico (Wei-Haas, 2017). Liquefaction is defined by a loss of shear strength of soil due to a sudden increase in the excess pore-water pressure (EPWP) caused by the presence of a rapid dynamic load (e.g., earthquake).

According to the principles of continuum mechanics, the transmission of waves through soil can be classified into three distinct categories: P waves (pressure or primary waves) and S waves (shear or secondary waves) (Nakagawa et al., 1997; Steeb et al., 2014). P waves are the strongest wave and have a greater velocity than S waves. The P-wave velocity (V_p) is shown to reach a maximum value of 1500 m/s (4921 ft/s) in water. P waves in saturated soils are created by the compression and dilation movement of both the soil skeleton and the pore fluid (Leong et al., 2016). The S wave travels through only the soil skeleton, creating a shearing motion rather than a compression motion. This shearing motion induces deformations in the soil, altering the flow path of water and leading to an increase in pore-water pressure (PWP). Simultaneously, this process reduces the shear strength of the soil, resulting in liquefaction.

Research on soils susceptible to liquefaction, such as loosely packed, fine, water-saturated sands, demonstrated that liquefaction depends on several governing factors such as earthquake intensity and duration, groundwater depth, soil characteristics (e.g., plasticity, particle shape, i.e., rounded versus angular, placement conditions, drainage conditions, historical conditions, e.g., older soils that have previously subjected to cyclic shearing), and if a building load is present (Bolt, 1993). However, all these parameters are interconnected with or govern the rate at which water dissipates. When water does not have enough time to dissipate during a rapid enough dynamic load, a net increase in the pore-water pressure (PWP) is observed—referred to as EPWP (Ueng et al., 2017)—, and the effective stress ($\sigma' = \sigma - u$, kPa) approaches zero. Here, σ is total stress, σ' is effective stress, and u is PWP.

Conventional approaches for mitigating liquefaction involve dynamic compaction, stone columns, and compaction piles, to name a few. The goal is to increase shear strength of the soil and often referred to as ground-improvement work. However, these methods are time-consuming, costly, and require verification of their effectiveness. Alternatively, researchers are investigating the effects of altering hydraulic conductivity or increasing shear strength to mitigate liquefaction. Such practices include decreasing EPWP, microbially induced-calcite precipitation (MICP), induced partial saturation (IPS).

A potential theory, introduced by our research team, is that electromagnetic (EM) waves can increase hydraulic conductivity of a noncohesive soil. Electromagnetic waves have traditionally been used for radar-based geophysical detection and characterization, and even remediation (Farid et al., 2019; Azad et al., 2015), as electrostatic sources and alternating electric fields can align individual water molecules and magnetic fields can

float droplets of water (Ikezoe et al., 1998). EM waves are generated when electric and magnetic fields alternate orthogonally to each other and the direction of wave propagation. These waves can polarize material and impact electric properties of the medium, such as the dielectric properties of water. According to Sun et al. (2007), when water is under the influence of an electric field, water molecules can start to reorient and align parallel to the direction of the electric field. As reorientation occurs, the hydrogen bonds potentially weaken, thus decreasing the viscosity of the molecule. A decrease in the viscosity of the permeant fluid—water here—potentially results in an increase in hydraulic conductivity.

The following research is broken into two studies. The first study investigates the impact of radio frequency (RF) waves at varying power levels and frequencies on the hydraulic conductivity of noncohesive soils such as sandy soils.

The second study explores the correlation between hydraulic conductivity and EPWP buildup, assesses the influence of electromagnetic (EM) waves on EPWP buildup through the alteration of hydraulic conductivity, and evaluates the potential of EM-induced mitigation of liquefaction.

CHAPTER TWO: ELECTROMAGNETIC WAVES IMPACT ON HYDRAULIC CONDUCTIVITY OF GRANULAR SOILS

Abstract

Electromagnetic (EM) waves are used for various purposes such as geophysical nondestructive detection and characterization. Like any measurement tool, EM waves impact properties that need to be measured. Various power levels and frequencies of EM waves impact the hydraulic conductivity of various soils differently. This increases the number of potential applications of EM waves such as contamination remediation. This paper describes the effects of radio frequency (RF) EM waves on the hydraulic conductivity of glass beads and natural sand. A series of tests were conducted using a customized, rigid-wall, cylindrical permeameter placed inside a resonant cavity made of Plexiglas covered with electrically conductive transparent films. Constant head (D2434, ASTM, 2006) tests were performed to measure the hydraulic conductivity of the samples. RF stimulation was performed using a magnetically coupled loop antenna at a constant frequency of 726 MHz and input power levels of 10, 25, 40, and 50 Watts. The hydraulic conductivity of both natural sand and glass-bead samples increased with RF stimulation, and the increase was larger at higher RF power. At 40 Watts, the hydraulic conductivity of the glass-bead sample increased by 8.7% of the unstimulated value, whereas that of the natural sand increased by 25.4%. Furthermore, measurement of the electric-field component of RF waves was also performed to find and illustrate the pattern of the electric field to facilitate the evaluation of the RF impact on hydraulic conductivity. The

electric field was also simulated using COMSOL Multiphysics and validated against the experimentally measured electric field. A finite-difference numerical model was developed in MATLAB to analyze the seepage flow, which was then validated against the experimentally measured hydraulic conductivity to determine the spatial variation of the hydraulic head within the soil specimen. An optimization scheme was then used to develop a governing equation for the RF impact on hydraulic conductivity.

Introduction

Seismic-induced liquefaction is a result of a sudden increase in the excess pore-water pressure (EPWP) in loose, water-saturated noncohesive soils. This phenomenon has been observed in many different earthquakes such as the 1964 Niigata, Japan (Kramer, 1996), 1999 Adapazari, Turkey (Martin et al., 2004), and 2011 Christchurch, New Zealand (Cole et al., 2012) earthquakes. Liquefaction leads to a reduction of effective stress and a decrease in contact force between the soil grains, often resulting in the loss of shear strength, thus, lateral spreading, slope instability, and foundation and building damage.

Research on soils susceptible to liquefaction, such as sand and silty sand, demonstrated that liquefaction depends upon parameters such as peak acceleration, groundwater level, soil's grain size, relative density, cyclic shear strength, soil's plasticity, and degree of water saturation (Kramer, 1996). All these parameters, however, are linked to the water dissipation rate. The inability of fluids to fully dissipate in a short period of an earthquake leads to a rapid buildup of excess pore-water pressure (EPWP), resulting in liquefaction. Nonetheless, if all soil properties remain constant, liquefaction depends upon fluid properties. Using a viscous fluid ($k = 0.0021 \text{ cm/s}$) in a centrifuge

test, Sharp et. al. (2004) successfully demonstrated a decrease in the thickness of the liquified layer and settlement with an increase in permeability. Grainey et al. (2012) obtained a lower EPWP ratio (r_u), which is a ratio between the excess pore-water pressure and initial effective stress and a smaller thickness of liquified soil and shear strain when the tests were conducted using water than the one that was conducted using more viscous fluids (hydraulic conductivity was 25 times lower than water).

Electromagnetic waves have traditionally been used for radar-based geophysical detection and characterization, and even remediation (Farid et al., 2019; Azad et al., 2015) as electrostatic sources can align individual water molecules and magnetic fields can float droplets of water (Ikezoe et al., 1998). By the same token, water dipoles oscillate in alternating electromagnetic (EM) fields. The vibration of water molecules enhances different transport mechanisms inside the soil, therefore altering hydraulic conductivity. Azad et al. (2014) conducted a study using radio frequency (RF) waves to alter hydraulic conductivity. In sandy soils, hydraulic conductivity increased as much as 14% when an RF test was conducted on natural sand at a frequency of 153 MHz with an RF-power input of 20 Watts. The increase in hydraulic conductivity was justified by the RF energy absorbed by the water molecules, which decreased viscosity and led to an increase in hydraulic conductivity. This is important because using electromagnetic waves reduces soil susceptibility to liquefaction by reducing hydraulic conductivity related to liquefaction. A reduction of even the slightest amount of generated EPWP can mitigate liquefaction. Therefore, the objectives of this study were to investigate (1) RF waves on the hydraulic conductivity of sandy soils and (2) determine whether this could be sufficiently large and fast enough to reduce excessive pore-water pressure (EPWP)

during earthquakes to mitigate liquefaction. During earthquakes, EPWP is generated within fine sands or silty sands due to a low dissipation rate. To achieve these stated goals, the effect of RF waves at varying powering levels and frequencies on the hydraulic conductivity of noncohesive soils were studied as well as measuring the increase in the EPWP within non-cohesive soils during unstimulated and RF-stimulated tests at different RF waves' frequencies and power levels.

Theoretical Background

Hydraulic Conductivity

Water seeps through the void space between soil grains that form interconnected paths. Seepage flow and its velocity are measured by and depend on hydraulic conductivity. Water flows through the soil from one point to another when there is a difference in the total head (also known as hydraulic head). In this paper, we assume seepage flow is governed by Darcy's Law, i.e., for flow from Point A to Point B,

$$Q = vA = \left(-k \frac{dh}{dL}\right)A \quad (1)$$

where Q = discharge (m^3/s), h = total head (m), $dL \equiv$ flow-path length (m), A = cross-sectional area of the soil specimen (m^2), k = hydraulic conductivity of soil (m/s), v = discharge or Darcy's velocity (m/s), and $\frac{dh}{dL}$ = hydraulic gradient.

The hydraulic conductivity of soils is a function of the property of both the porous medium (i.e., intrinsic permeability) and fluid (unit weight and viscosity) (Hubbert, 1957).

$$k = \frac{K\gamma}{\mu} = \frac{Kg}{\nu} \quad (2)$$

where K = intrinsic permeability of a soil medium (m^2), which depends on the shape of openings and the mean-pore diameter (Fetter, 2001) of the soil; g = gravitational acceleration (m/s^2); γ = unit weight of water (N/m^3); μ = absolute or dynamic viscosity of water ($\text{Pa}\cdot\text{s}$); $\nu = \frac{\mu}{\rho}$ = kinematic viscosity (m^2/s); ρ = density water (kg/m^3). Typical values of intrinsic permeability and hydraulic conductivity of different soils are presented in Table 1.

Table 1 Ranges of Intrinsic Permeability and Hydraulic Conductivity for Unconsolidated Sediments (Fetter, 2001)

Material	Intrinsic Permeability (Darcy's)	Hydraulic Conductivity (cm/s)
Clay	$10^{-6} - 10^{-3}$	$10^{-9} - 10^{-6}$
Silt, sandy silts, clayey sands, till	$10^{-3} - 10^{-1}$	$10^{-6} - 10^{-4}$
Silty sand, fine sand	$10^{-2} - 1$	$10^{-5} - 10^{-3}$
Well-sorted sands, glacial outwash	$1 - 10^2$	$10^{-3} - 10^{-1}$
Well-sorted gravel	$10 - 10^3$	$10^{-2} - 1$

This research work hypothesizes that by impacting the permeating fluid, in this case, water, the hydraulic conductivity can be altered without the need to change the intrinsic permeability via costly and permanent methods of changing the soil environment, e.g. compaction.

Liquefaction

Liquefaction occurs when the shear strength of saturated loose soils is lost due to the sudden increase in the pore-water pressure (PWP, u) beyond the hydrostatic PWP—referred to as excess pore-water pressure (EPWP, u_e)—due to a rapid dynamic load of an earthquake. During rapid loading, there is a sudden increase in EPWP, thus decreasing the amount of time for PWP to dissipate. As a result, the effective vertical stress of the soil decreases to zero, leading to liquefaction. The vanishing effective vertical stress leads to the loss of friction, the sole source of shear strength in noncohesive soils, such as sand.

Liquefaction susceptibility depends upon a number of factors, including geologic and compositional properties as well as the state of the soil, since volume-change behavior influences the rise of EPWP. Liquefaction has been dominant in soils that have shallow groundwater depths. Moreover, reclaimed lands with loose soil are prone to liquefaction (Kramer, 1996). Liquefaction is not common in all types of soils. Fine-grained soils such as clay have cohesion, and very coarse-grained soils, though frictional, are highly permeable, hence, both are less susceptible to liquefaction. However, liquefaction of nonplastic silts have been observed (Kramer, 1996). Nonplastic and cohesionless silts having dimensions equal in all directions (bulk shape) are prone to liquefaction (Kramer, 1996). In the case of the Adapazarı earthquake, the layer of sand containing 30% nonplastic fines and classified as silty sand (SM) was considered liquefiable under moderate levels of ground shaking (Martin et al., 2004) and liquefied in areas where soil treatment was not completed. Liquefaction of soil also depends upon the gradation of soil. Well-graded soils are less prone to any increase in EPWP than poorly graded or uniformly graded soils. An increase in the pore-water pressure during

earthquakes also depends upon the density of the soil and its initial stress condition (Kramer, 1996)

An EPWP ratio parameter, $r_u = \frac{\Delta u}{\sigma'}$, has been defined to illustrate the path toward liquefaction, where σ' = initial effective stress, and $\Delta u = u_e$ = EPWP increase during an earthquake. When $r_u = 1$, liquefaction occurs, and when $r_u = 0.25$ to 0.70 , partial liquefaction occurs (Ganainy et al., 2012).

The EPWP generation has a significant effect on the shear strength, stability, and settlement characteristics of soil deposits, even if the soil does not completely liquefy (Hazirbaba and Rathje, 2009). Therefore, an even small decrease in the EPWP can reduce the potentially hazardous effects of liquefaction.

Electromagnetic Waves

Alternating electric fields generate magnetic fields, and vice versa, alternating magnetic fields generate electric fields. Electromagnetic (EM) waves are formed when an electric and magnetic field alternate perpendicular to each other and the direction of wave propagation. These orthogonal oscillations are governed by Maxwell's equations. Maxwell's equations are a set of four equations, written in either integral or differential form, stating the relationship between the fundamental electromagnetic quantities. The fundamental quantities are the electric flux density, \vec{D} (C/m²), the magnetic flux density, \vec{B} (Wb/m²), the electric field intensity, \vec{E} (V/m), the magnetic field intensity, \vec{H} (A/m), the current density, J (A/m²), and the electric charge density, ρ (C/m³) (Santamarina et al., 2001). For general time-varying fields, Maxwell's equation can be written as follows.

$$\vec{\nabla} \cdot \vec{D} = \rho \quad (3)$$

$$\vec{\nabla} \cdot \vec{B} = 0 \quad (4)$$

$$\vec{\nabla} \cdot \vec{E} = -\frac{\partial \vec{B}}{\partial t} \quad (5)$$

$$\vec{\nabla} \times \vec{H} = \vec{J} + \frac{\partial \vec{D}}{\partial t} \quad (6)$$

EM Waves Impact on Soil Media

Soils have three phases: (i) solid grains with voids filled with (ii) air and/or (iii) fluids that have different physical and dielectric properties. A dielectric is a material that can be polarized by an EM wave. Water has a high dielectric permittivity ($\gg 80$). Oscillations of individual water molecules can induce a net change in the movement and flow of water through a porous medium without altering the properties of the medium itself (Azad et al., 2014). When under the influence of an electric field, water molecules can start to reorient parallel to the direction of the electrostatic field (Sun et al., 2007). As reorientation occurs, the hydrogen bond starts weakening, thus decreasing the viscosity of the molecule. A decrease in viscosity could result in an increase in hydraulic conductivity.

Methodology

In order to study the impact of EM waves on hydraulic conductivity, spatial and temporal relations between both seepage and electric fields need to be studied. Experimental measurements do not provide a complete three-dimensional image of the two. To acquire a complete picture, experimentally validated numerical models are

needed. The following is an explanation of how the two numerical simulations were generated and experimentally validated.

The 3D Numerical Model of Seepage Flow developed in this research simulates a saturated medium and flow governed by the conservation of mass.

$$\frac{\partial \rho}{\partial t} + \vec{\nabla} \cdot (\rho \vec{v}) = 0 \quad (7)$$

where ρ = fluid density (m³/s), t = time (s), and \vec{V} = seepage flow velocity vector. In the case of incompressible fluids, the density of the fluid is constant. Therefore, the conservation of mass equation (Equation 7) can be simplified to the conservation of volume equation.

$$\vec{\nabla} \cdot v = 0 \quad (8)$$

Applying Darcy's Law, $\vec{v} = -k\vec{i}$ wherein 3D $\vec{i} = \vec{\nabla}h = \frac{\partial h}{\partial x}\vec{i} + \frac{\partial h}{\partial y}\vec{j} + \frac{\partial h}{\partial z}\vec{k}$,

Equation 8 can now be rewritten as follows.

$$\vec{\nabla} \cdot \vec{v} = - \left\{ \frac{\partial}{\partial x} \quad \frac{\partial}{\partial y} \quad \frac{\partial}{\partial z} \right\} \begin{bmatrix} k_{xx} & k_{xy} & k_{xz} \\ k_{yx} & k_{yy} & k_{yz} \\ k_{zx} & k_{zy} & k_{zz} \end{bmatrix} \left\{ \begin{array}{c} \frac{\partial}{\partial x} \\ \frac{\partial}{\partial y} \\ \frac{\partial}{\partial z} \end{array} \right\} h = 0 \quad (9)$$

The flow is also simulated experimentally using a rigid-wall constant-head test, according to ASTM D2434 (ASTM, 2006), where the flow rate of water is high, and a constant head can be maintained by a continuous supply of water. For a homogeneous soil sample, if there are no EM waves, then hydraulic conductivity can be assumed spatially constant.

$$k = - \frac{V}{t} \frac{L}{A\Delta h} \quad (10)$$

where, $\Delta h = h_L$ = hydraulic head loss across the soil medium (m), A = cross-sectional area of soil specimen (m^2), L = length of soil specimen (m), t = time of water collection (s), and V = volume of water collected (m^3).

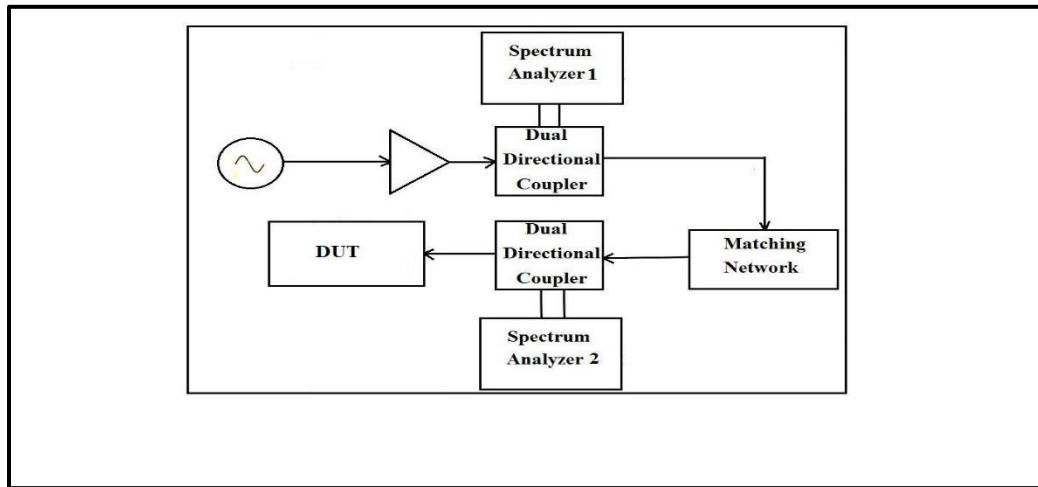
Experimental Setup and Testing Procedures

The following are the details on a series of tests that evaluated the impact of RF stimulation on the hydraulic conductivity of granular soils, which includes details of RF wave generation and hydraulic conductivity measurements.

RF Wave Setup

To supply the power and RF electric field intensity for these tests, a magnetically coupled loop antenna, inserted into the cavity parallel to the magnetic lines, was used. The loop antenna was made of an RG-8 coaxial cable. The RF signal was generated using the Agilent Model #E4400B signal generator. An amplifier was used to amplify the generated signal. To maximize power output and reduce harmful reflections back into the amplifier, the impedance of the load (setup) should match that of the source (50Ω). The impedance was measured using an Agilent N9320A, vector network analyzer (VNA), and matched to the 50Ω impedance of the RF source using a matching network made of a series of variable capacitors. Two dual-directional couplers were also used in the network to monitor the forward power into the device under testing (DUT) and the reflected power back into the amplifier.

Figure 1 Shows the Schematic of the Setup Used for Launching RF Into the DUT.



All these tests were performed on a resonant cavity filled with two types of medium, one filled with glass beads and the other filled with a natural sand sample. The saturated glass-bead specimen was prepared using the wet-pluviation method (Kuerbis and Vaid, 1988). Glass beads for this study are Class-A Ballotini impact beads with a specific gravity of 2.46 g/cm^3 . Table 2 displays the properties of the beads.

Table 2 Properties of Glass Beads (Najafi, 2014)

Designation	Potters Number	U.S. Sieve	Maximum Size (in.)	Minimum Size (in.)	Maximum Size (μm)	Minimum Size (μm)	Minimum % of Round
Class A	20-30		0.0331	0.0234	850	600	65

A customized experimental setup to measure RF-stimulated hydraulic conductivity was developed here. Glass beads and natural sand were used as the coarse-grained samples in this test. The natural sand was classified as SW, according to the

USCS classification system. The properties of the glass beads used are presented in Table 2.

To perform the hydraulic conductivity tests, a customized, rigid-wall, cylindrical permeameter was constructed using acrylic material. However, prior to performing the test using the customized permeameter, the customized device needed to be calibrated. Hence, the unstimulated tests were performed using both a standard permeameter (2.5-inch diameter and 12-inch height) as suggested by D2434 (ASTM, 2006) and the customized (152-mm diameter and 140-mm height) permeameter to calibrate the customized permeameter. Figure 2 displays the schematic of the customized, rigid-wall, cylindrical permeameter setup. The glass beads used in this test were prepared by dry-pluviation. The total density of the glass-bead sample was measured to be 14.72 kN/m^3 . In the case of the natural sand, natural sand was poured into the permeameter in three layers. Each layer was compacted using 50 blows with a standard compaction hammer. The density of the natural sand was measured to be 18.25 kN/m^3 . The depth of the soil specimen in the customized permeameter was 110 mm. Figure 2 shows the schematic of the setup and its dimensions, and Figure 3 shows the setup for the RF-stimulated hydraulic conductivity test. The customized permeameter was placed inside a $490\text{mm} \times 390\text{mm} \times 390\text{mm}$ resonant cavity. RF stimulation was performed on both the glass-bead and natural sand samples at a frequency of 726 MHz and power levels of 10, 25, and 40 Watts.

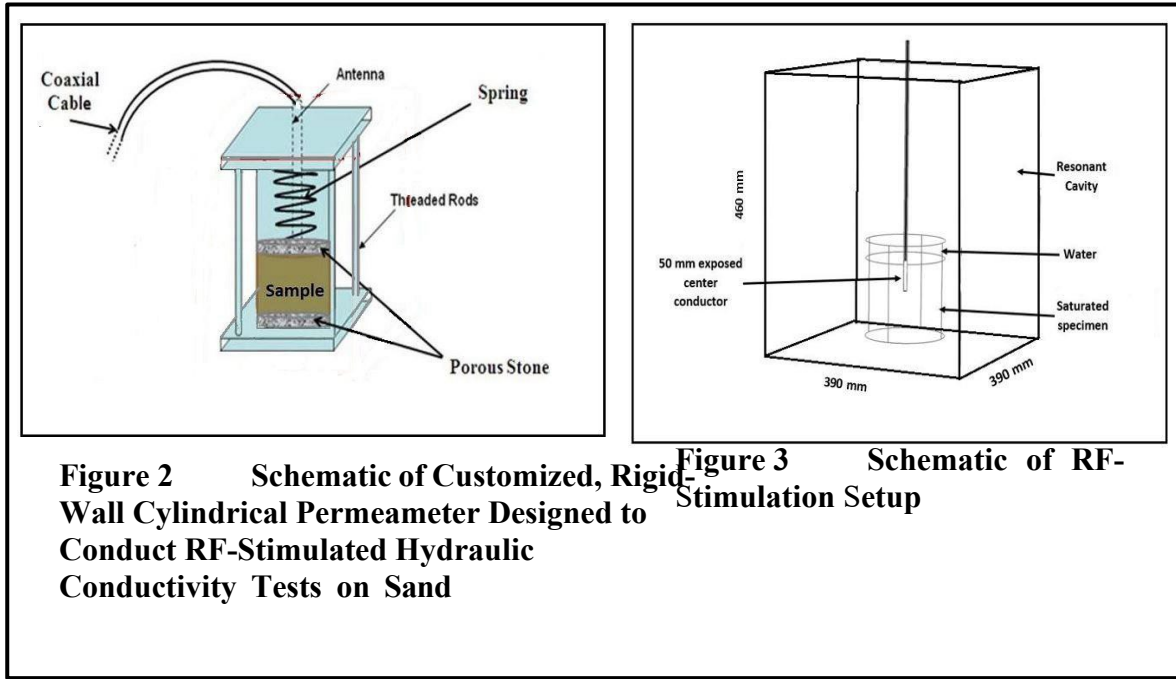
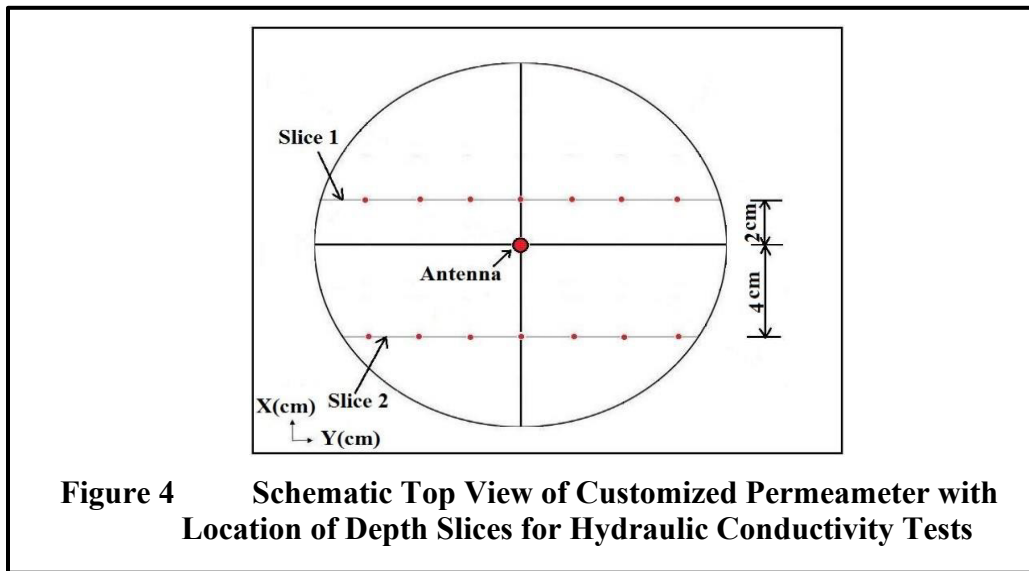


Figure 2 Schematic of Customized, Rigid-Wall Cylindrical Permeameter Designed to Conduct RF-Stimulated Hydraulic Conductivity Tests on Sand

Figure 3 Schematic of RF-Stimulation Setup

Electric Field Mapping

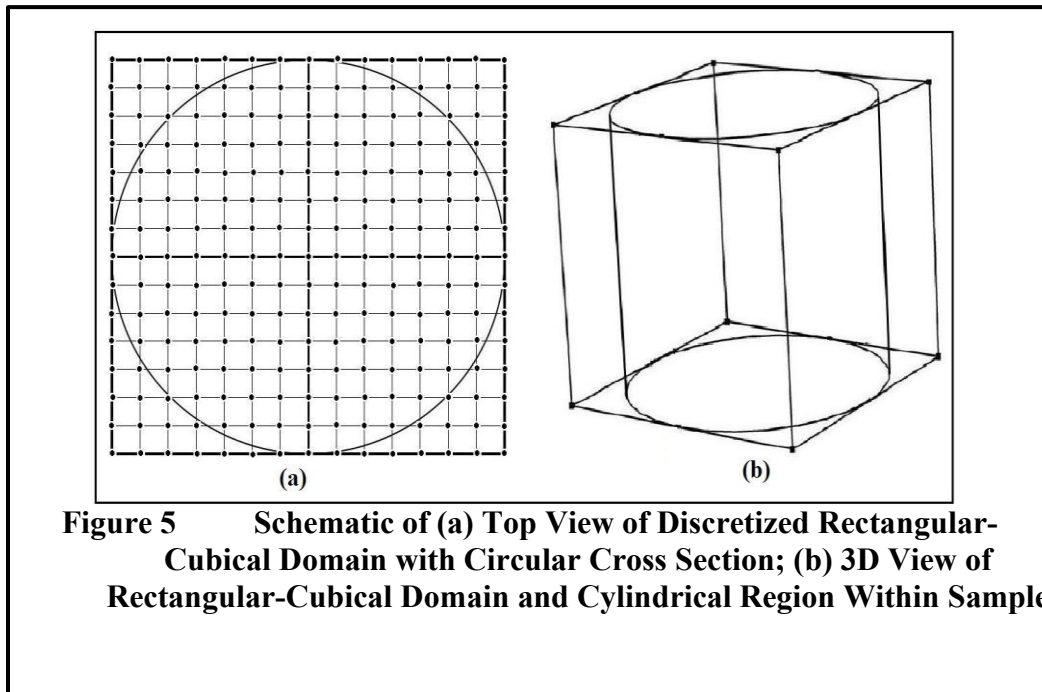
Using a vertical monopole probe, the electric field inside the cavity was measured. Using an RG-58, 18 GHz precision-test cable, the monopole probe was connected to a spectrum analyzer to measure the electric field at the corresponding location of the probe inside the cavity. The probe was moved to various locations throughout the specimen as a number of holes were drilled through the top plate of the resonant cavity on a 2cm × 2cm grid in the X-Y plane. The monopole was placed inside a glass tube casing and inserted vertically into the cavity. The location of the probe on the top decided the respective X- and Y-coordinates of the probe and the depth of the insertion decided the Z-coordinate.



Electric-field measurements for the RF-stimulated hydraulic conductivity tests were performed at frequencies of 710 MHz and 726 MHz. The location of the measurement probe along the X-direction was fixed at distances of 2cm and 4cm from the centrally placed source (monopole antenna). A total of seven measurement points along the Y-axis were selected, which were separated at 2cm intervals. Figure 4 presents the schematic top view of the customized permeameter with the location of the depth slices. Measurements were recorded in dBm using the spectrum analyzer at the frequency generated by the signal generator. The electric field was also numerically simulated using the RF module of COMSOL Multiphysics and validated against the experimentally measured electric field.

3D Numerical Forward Model of Seepage for Hydraulic Conductivity Tests

A 3D numerical model of seepage flow was also developed in the MATLAB interface using the finite-difference method. This model was used to correlate the RF field with the change in hydraulic conductivity due to RF stimulation. The water-saturated soil specimens were 15cm in diameter and 11cm in height. The entire grid used to model the flow was a rectangular-cubical specimen with the dimensions of 15cm \times 15cm \times 11cm. This rectangular- cubical domain was discretized into 15 nodes along both the X and Y axes. The top view of the discretized domain has a circular cross-section and rectangular mesh, which is illustrated in Figure 5. The top and bottom surfaces of the cylindrical specimen were modeled as Dirichlet boundary conditions with known hydraulic heads. However, the circumference of the permeameter was an impermeable boundary and was modeled using Neuman boundary conditions.



The computational code was developed based on the central finite- difference method and then used to calculate the spatial variation of the hydraulic head within the soil using the hydraulic conductivity values obtained for the unstimulated tests. Equation 9 was used, and the flow through the soils was considered at the steady-state for the unstimulated tests. Furthermore, the flow and discharge rates were also calculated. However, this only solved the hydraulic head inside the specimen while the test was performed in the unstimulated condition.

The hydraulic head under RF stimulation was assumed to be k' , and $\vec{V} = -k'\vec{\nabla}h$ for flow was rewritten as:

$$\vec{\nabla} \cdot \vec{V} = - \left\{ \frac{\partial}{\partial x} \quad \frac{\partial}{\partial y} \quad \frac{\partial}{\partial z} \right\} \begin{bmatrix} k'_{xx} & k'_{xy} & k'_{xz} \\ k'_{yx} & k'_{yy} & k'_{yz} \\ k'_{zx} & k'_{zy} & k'_{zz} \end{bmatrix} \begin{Bmatrix} \frac{\partial}{\partial x} \\ \frac{\partial}{\partial y} \\ \frac{\partial}{\partial z} \end{Bmatrix} h = 0 \quad (11)$$

$$\text{where, } k' = \begin{bmatrix} k'_{xx} & k'_{xy} & k'_{xz} \\ k'_{yx} & k'_{yy} & k'_{yz} \\ k'_{zx} & k'_{zy} & k'_{zz} \end{bmatrix} \text{ is the RF-stimulated hydraulic}$$

conductivity tensor.

Since the application of RF waves had demonstrated altering hydraulic conductivity, it was proposed that RF-stimulated hydraulic conductivity (k') and the flow discharge (Q_{st}) in the RF-stimulated tests are functions of the electric field, E . Hence,

$$k' = f(E) \quad \& \quad Q_{st} = f(E) \quad (12)$$

Additionally,

$$s = \frac{E^2}{z_o} \text{ or } E = \sqrt{sZ_o} \quad (13)$$

$$P = s \times a \quad (14)$$

where, s = RF-power density (W/m²), Z_o = characteristic impedance of the free space (Ω), P = RF power (Watts), and a = area enclosing each node (m²).

From Equations 12, 13, and 14, it was proposed that the hydraulic conductivity and the flow discharge in the RF-stimulated tests are functions of the power density, and hence power. The results showed an increase in hydraulic conductivity with the increase of RF-power level in coarse-grained media. A nonlinear, but proportional, relation was assumed between the RF-stimulated hydraulic conductivity, k' , and RF power, P . Based on Equations 12, 13, and 14, the RF-stimulated hydraulic conductivity and RF-power can be correlated as follows.

$$k' = k + \beta\sqrt{P} \quad (15)$$

where β is a constant value, and k is the unstimulated hydraulic conductivity (cm/s).

Therefore, the increase in k' at each discretized node in the soil specimen domain could be correlated to the increase in the RF power at that node, while calculating the hydraulic head at the specific node. Equation 15 can be redefined as follows.

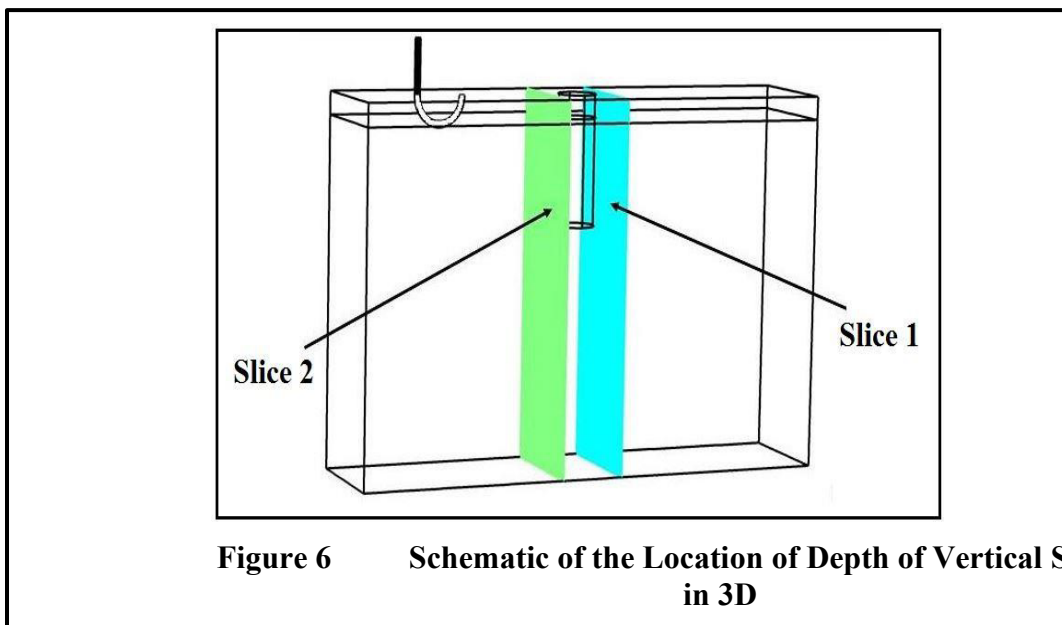
$$k' = k + \beta\sqrt{s \times a} \quad (16)$$

A similar computational code in the MATLAB interface was developed to solve Equations 11 and 16. The RF-power density at each node was obtained from the RF forward model generated using COMSOL Multiphysics. The RF-power densities in the

form of a 3D matrix were exported from the COMSOL model into the MATLAB interface. Afterward, an optimization scheme was implemented to find β by minimizing a cost function equal to the difference between the numerically simulated and experimentally measured values of the RF-stimulated discharge, i.e., $Q_{sim,st}$ $Q_{exp,st}$, respectively. The COMSOL code was used to export the RF-power densities at a frequency of 726 MHz at the power levels of 10, 25, and 40 Watts to be imported into the optimization scheme.

Results and Discussion

Electric-Field Measurement and Validation of Numerical Simulation



The electric-field pattern within the cavity numerically simulated using COMSOL was validated against experimentally measured values of the Z component of the electric field. This was because the vertically located monopole probe was vertically polarized, i.e., its measurement was dominated by the Z component of the electric field. The experimental measurements were performed at two frequencies, 498 MHz, and 632 MHz.

As seen in Figure 6, the experimental measurements were performed near where the pore-pressure transducer was installed within the sample. The location of Slice 1 is +4 cm away from the transducer along the X-axis, and Slice 2 is -4 cm along the X-axis.

Electric-field measurements were performed using a glass-cased monopole probe inserted into the cavity through the top plate down to the desired depth. Figures 7(A) to 7(D) show the maps of the experimentally measured electric field and numerically simulated E_z on Slices 1 and 2. Electric-field measurements are normalized to the maximum electric field measured on the corresponding slice.

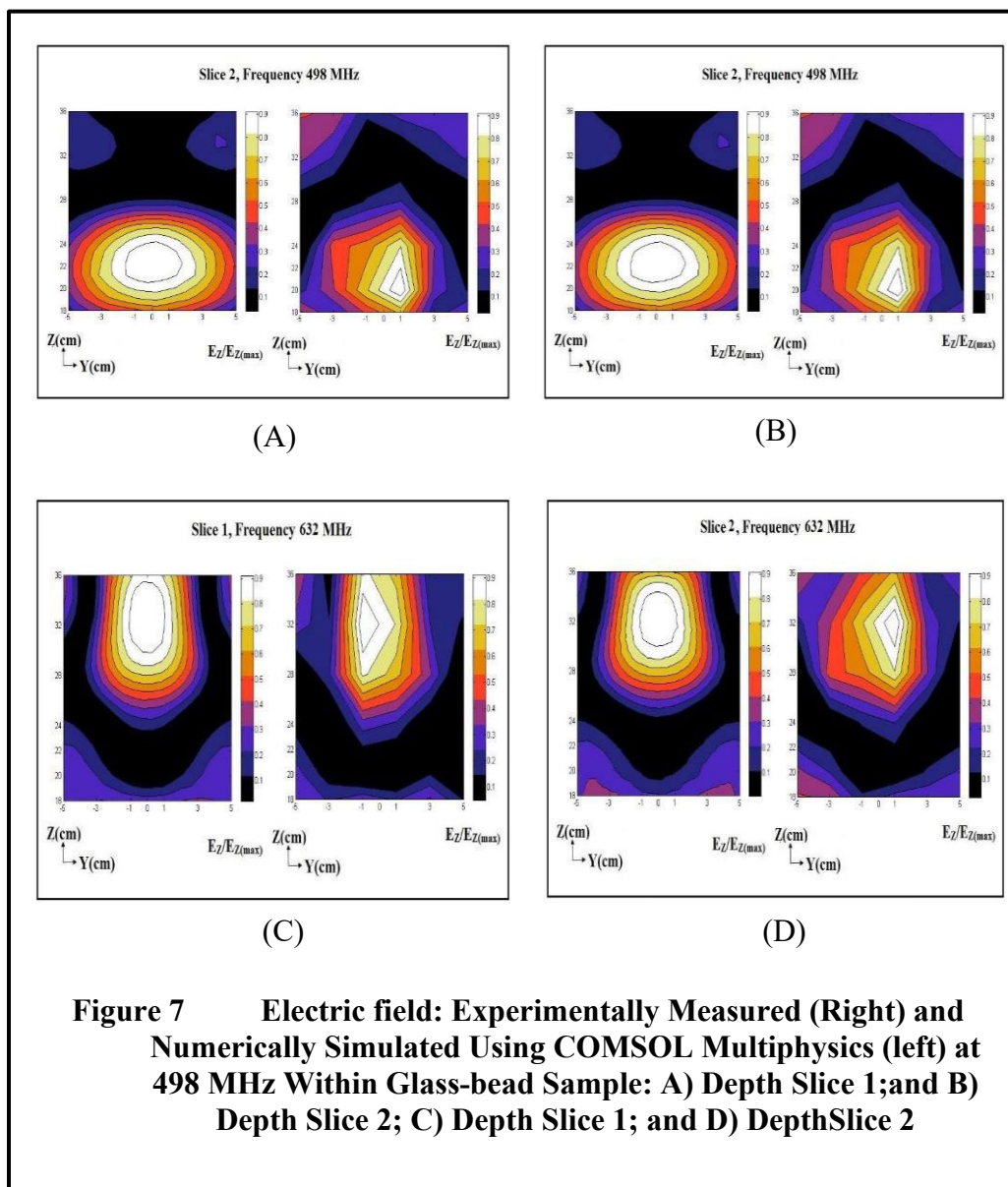
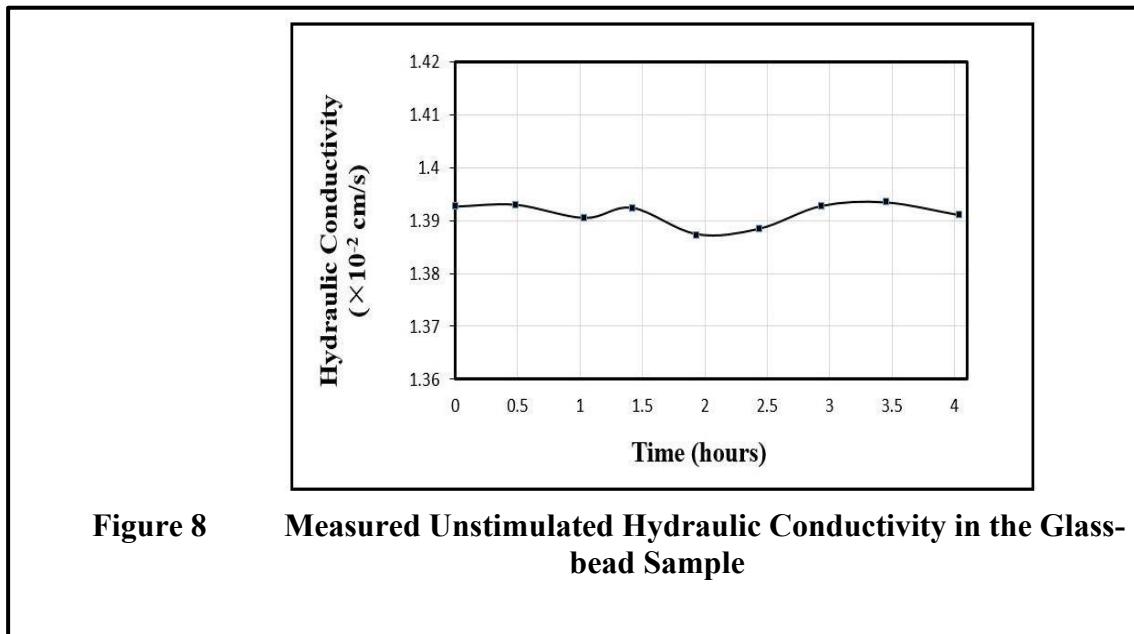
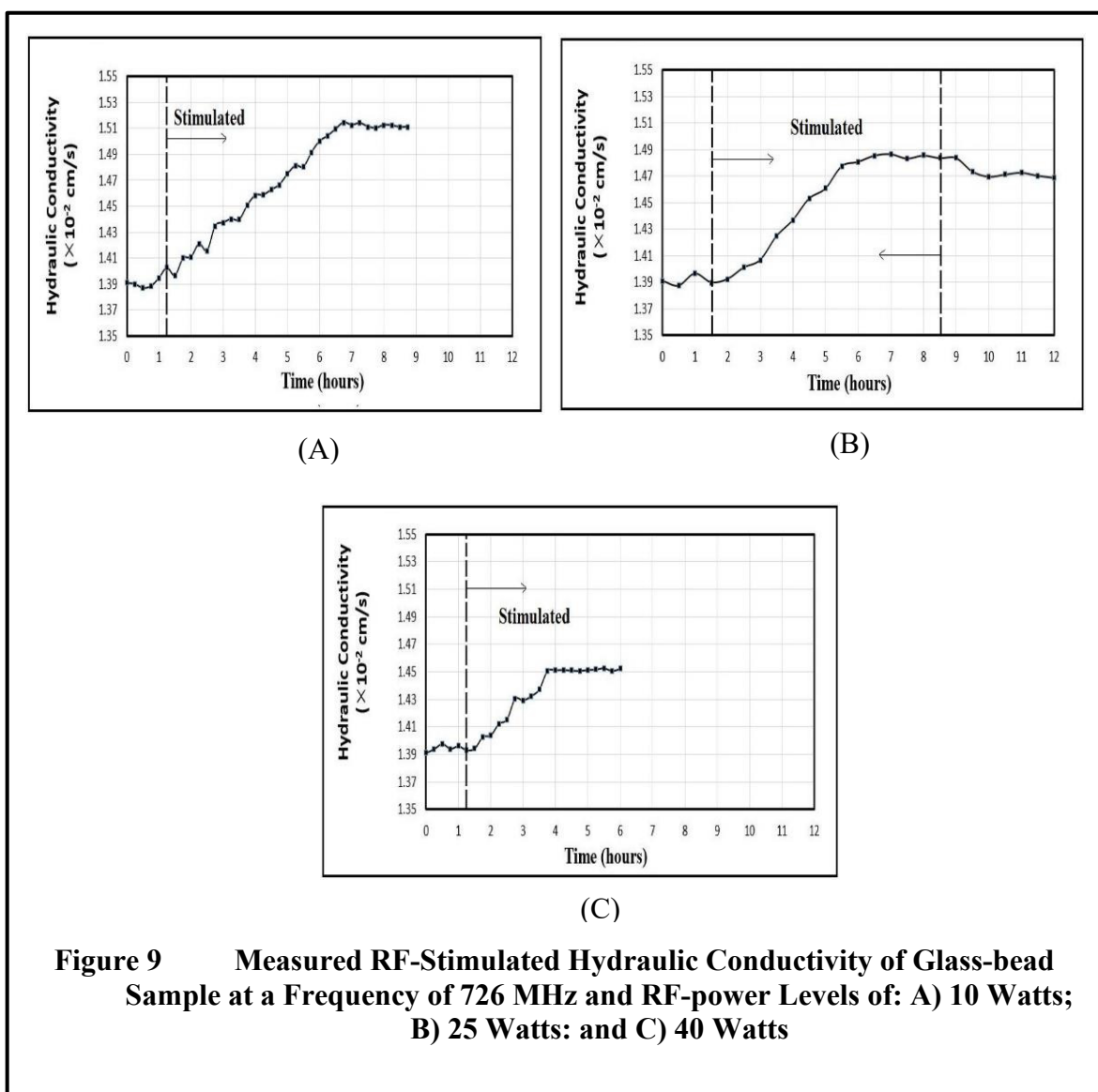


Figure 7 shows a reasonable agreement between the experimentally measured and numerically simulated electric fields on each slice. Since the monopole probe is not calibrated, the experimentally measured electric field does not represent the actual strength of the electric field within the cavity and just represents the electric field pattern. Both numerically simulated and experimentally measured electric-field patterns have their maximum at similar depths, i.e., the predesigned location of the pore-pressure transducer. As mentioned, the strength of the electric field at any specific location depends on the frequency of RF waves launched. Effects of RF waves on physical properties such as the viscosity of water may not be linear due to having different field patterns at different frequencies. Hence, a change in any physical property may or may not be linearly correlated with an increase or decrease of a frequency.

Hydraulic Conductivity Tests



RF waves' effect on hydraulic conductivity at different combinations of powers and frequencies needs to be studied. Figure 8 shows the measurement of the unstimulated hydraulic conductivity of the glass-bead sample performed using a standard permeameter. The test continued for four more hours. Hydraulic conductivity values remained fairly constant during the entire run of the test. The average unstimulated hydraulic conductivity of the glass-bead sample was measured to be 1.391×10^{-2} cm/s.



A series of RF-stimulated hydraulic conductivity tests were conducted on the glass-bead sample in the customized permeameter. There was a discrepancy of 3.5% between the customized permeameter and the standard permeameter. The discrepancy was calibrated out. To calibrate the customized permeameter, the hydraulic conductivity measurements obtained were multiplied with a multiplication factor of 1.035. The RF-stimulated tests were then conducted at a frequency of 726 MHz and RF-power levels of 10, 25, and 40 Watts. Figure 9 shows the hydraulic conductivity measurements at different RF-power levels. There was no sharp increase in the hydraulic conductivity with the RF stimulation. However, the hydraulic conductivity started to increase gradually with time and eventually attained a peak value. As seen in Figure 9(A), at an RF-power level of 10 Watts, hydraulic conductivity started to increase from 1.3942×10^{-2} cm/s to a peak value of 1.452×10^{-2} cm/s after two hours and 30 minutes and remained constant thereafter. Similar changes were observed at the other RF-power levels of 25 Watts and 40 Watts. At the RF-power level of 25 Watts, the RF stimulation was terminated once the RF-stimulated hydraulic conductivity reached its maximum. After the termination of RF waves, the hydraulic conductivity slightly decreased with time and then stabilized at a smaller value but was still larger than the unstimulated value. Even though the increase in hydraulic conductivity is larger at higher RF power levels, the slope of the increase is on average 0.0225% per hour and even seems higher for 10 Watts of power. The average unstimulated hydraulic conductivity before the start of RF stimulation and the peak value of the RF-stimulated hydraulic conductivity are compared in Table 3. As seen in Table 3, the hydraulic conductivity increased with the increase in

the RF input power. The increase in hydraulic conductivity was, however, small compared to the result obtained by Azad (2013).

Table 3 Hydraulic Conductivity Measurements of the Glass-Bead Sample at a Frequency of 726 MHz and Various RF-Power Levels

Power (Watts)	Average of Unstimulated Hydraulic Conductivity Measured Before RF- stimulation, k (cm/s)	RF-stimulated Hydraulic Conductivity, Peak Value, k' (cm/s)	Percent Change (%)
10	1.3942×10^{-2}	1.452×10^{-2}	(+) 4.190%
25	1.3911×10^{-2}	1.482×10^{-2}	(+) 6.864%
40	1.3923×10^{-2}	1.514×10^{-2}	(+) 8.774%

The effect of RF waves on hydraulic conductivity was smaller in glass beads than those for natural sand by Azad et al. (2014). Hence, a new set of RF- stimulated hydraulic conductivity tests were performed on the natural sand sample. Unstimulated hydraulic conductivity tests were first performed on the natural sand sample in the standard permeameter for calibration purposes.

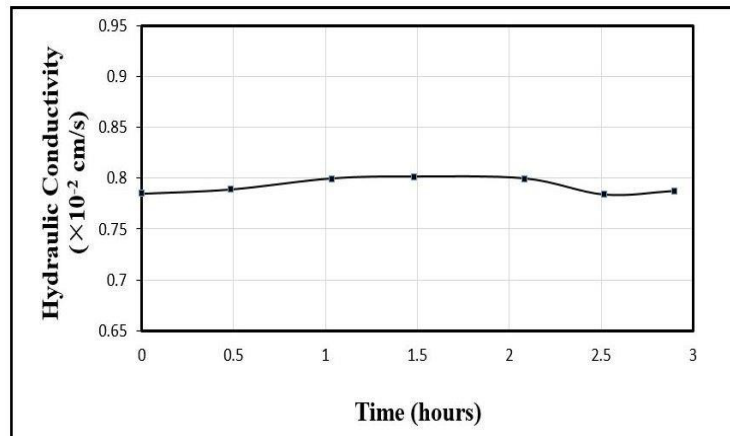
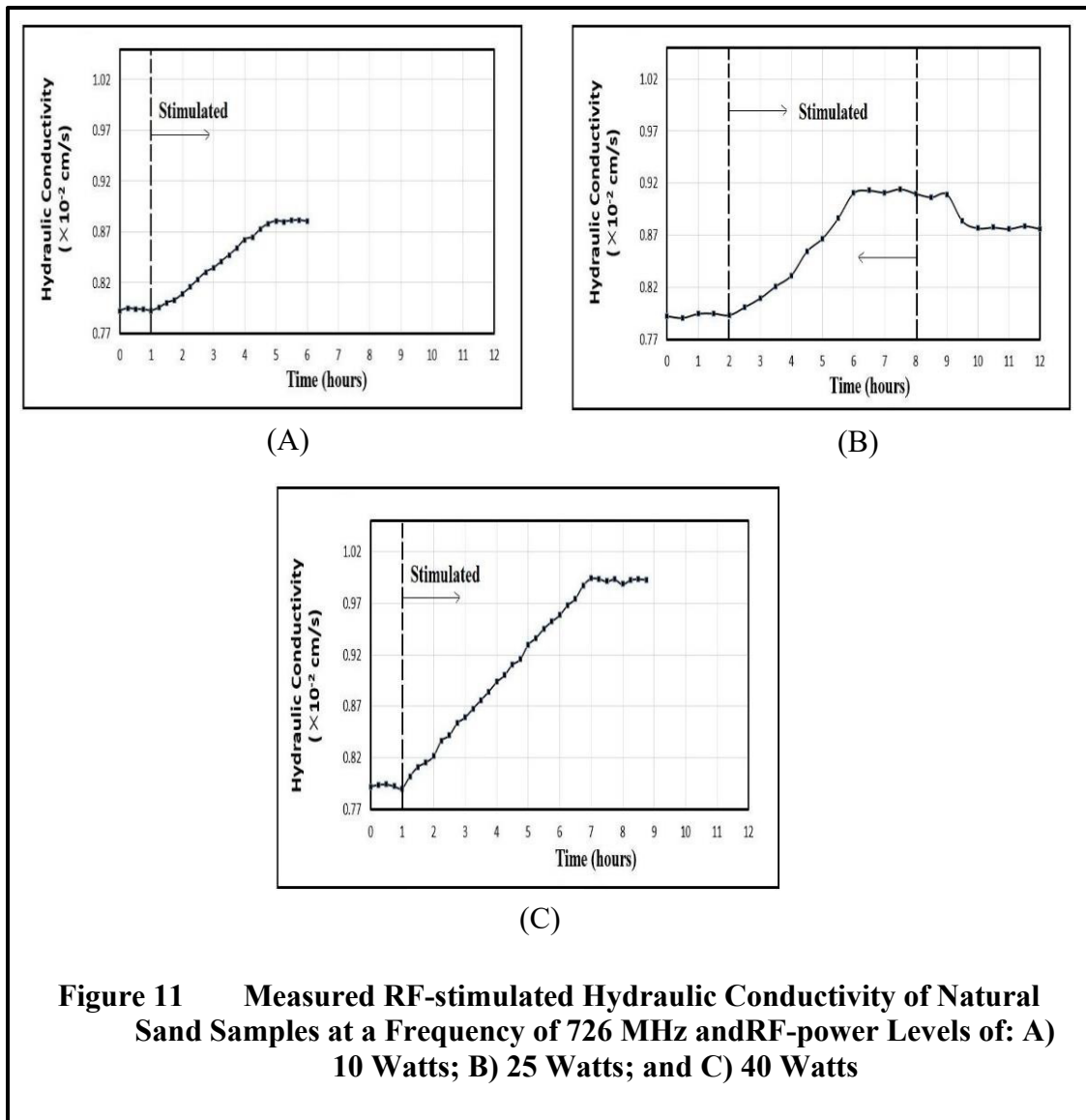


Figure 10 Measured Unstimulated Hydraulic Conductivity of a Natural Sand Sample

Figure 10 shows the measurement of unstimulated hydraulic conductivity of the natural sand sample performed using the standard permeameter. The average unstimulated hydraulic conductivity of the natural sand sample was measured to be 0.7924×10^{-2} cm/s. A series of RF-stimulated hydraulic conductivity tests were then conducted on the natural sand sample in the customized permeameter. There was a discrepancy of 5.1% between the customized and standard permeameters, which were later calibrated RF- stimulated tests were performed at a frequency of 726 MHz and power levels of 10, 25, and 40 Watts. The conducted tests were similar to the RF-stimulated hydraulic conductivity tests out on glass beads. Figure 11 shows the hydraulic conductivity measurements at different RF-power levels. The results show a similar pattern of the change in hydraulic conductivity. After RF stimulation started, the hydraulic conductivity of sthe and started to increase gradually with time and attained a peak value. At an RF-power level of 10 Watts, the hydraulic



conductivity started to increase from 0.7933×10^{-2} cm/s reached a peak value of 0.881×10^{-2} cm/s after four hours and remained constant thereafter. Similar changes were observed at other input powers of 25 and 40 Watts. At 25 Watts, RF stimulation was terminated once the RF-stimulated hydraulic conductivity of sand decreased with time and then stabilized at a slightly smaller value, yet much larger than the original unstimulated one. In the case of natural sand, not only is the increase in hydraulic conductivity larger at higher RF power levels, but the slope of the increase is also slightly

larger for higher RF power levels, increasing from 0.02% per hour for 10W to 0.03 and 0.033% per hour and even at 25 and 40 W.

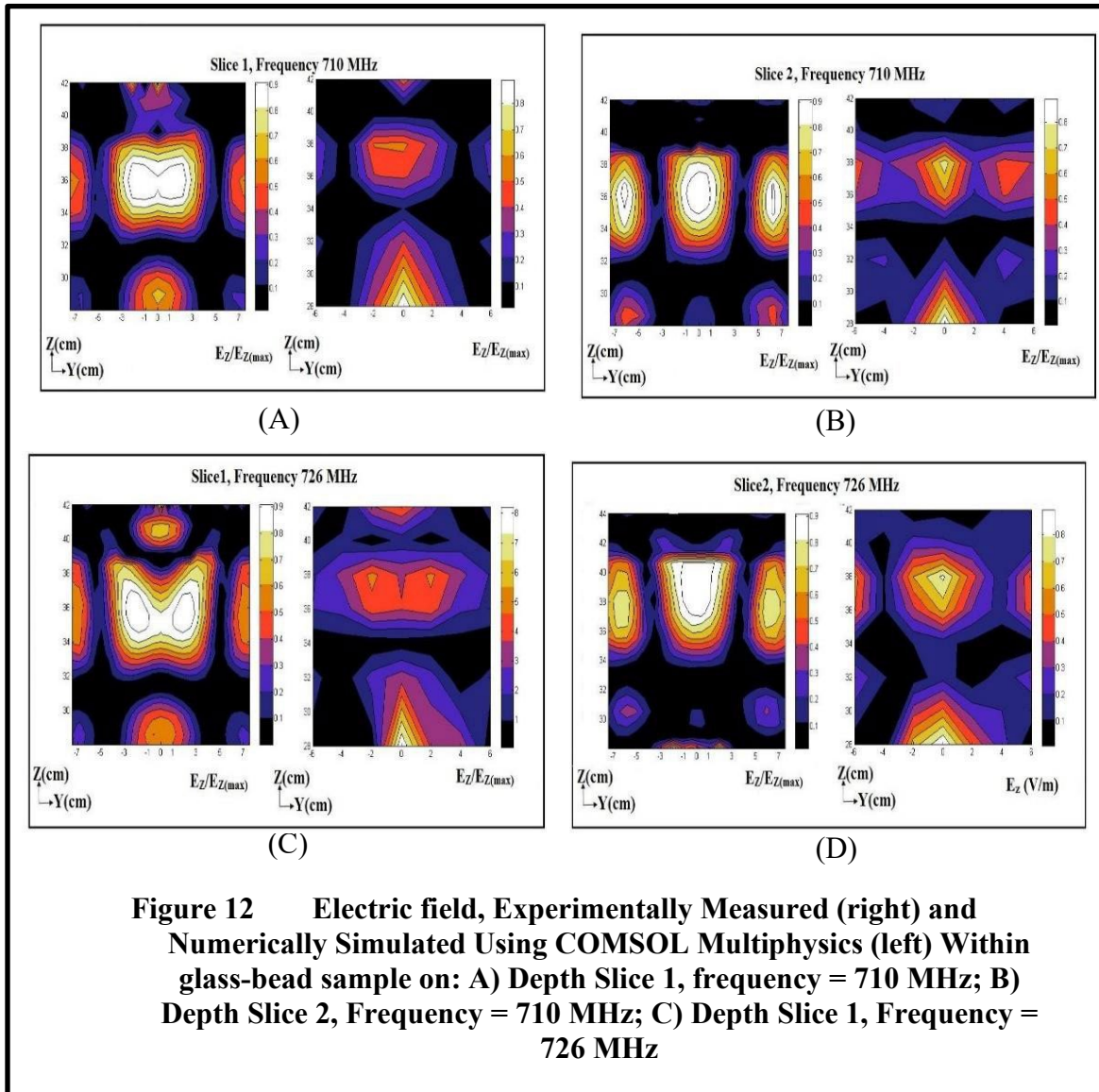
Moreover, the percent change in the hydraulic conductivity of natural sand due to RF stimulation is larger than that of the glass bead for all input RF-power levels. The results, however, show a similar pattern of increase and decrease in the hydraulic conductivity of both sand and glass beads during the application and termination of the RF stimulation, respectively. Table 4 summarizes the measurements between the unstimulated and RF-stimulated hydraulic conductivity. The increase in hydraulic conductivity was slow and gradual with the percent in change increasing at each increment of RF power level. With a test setup that can only provide up to 40 Watts of RF power, RF stimulation would not be high enough to change the hydraulic conductivity promptly, even for natural sand.

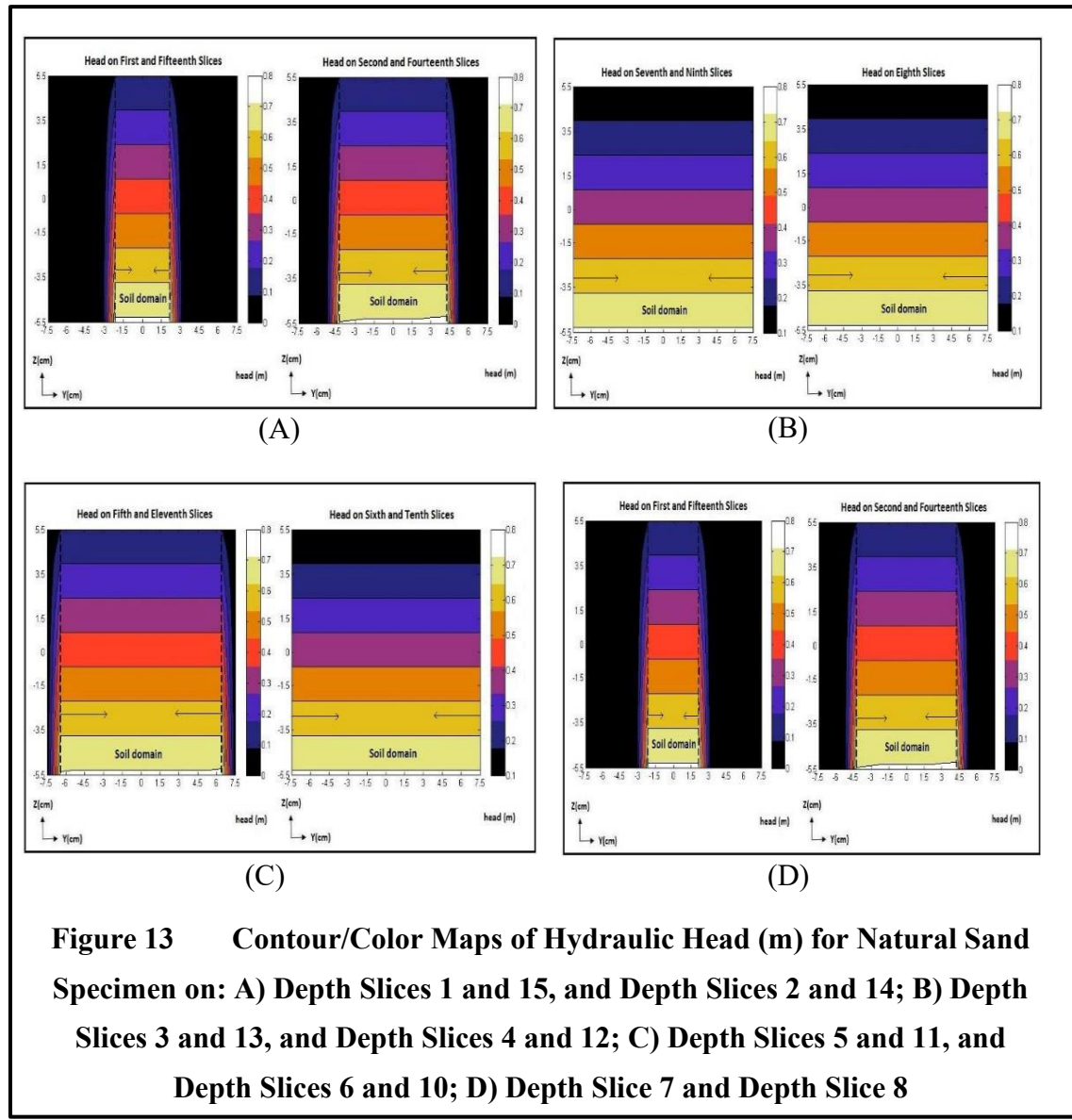
Table 4 Hydraulic Conductivity Measurements of the Natural Sand Sample at a Frequency of 726 MHz and Various RF-Power Levels

RF-Power (Watts)	Average of Measured Unstimulated Hydraulic Conductivity Values, k (cm/s)	RF-stimulated Hydraulic Conductivity, Peak Value, k' (cm/s)	Percent Change (%)
10	0.7933×10^{-2}	0.881×10^{-2}	(+) 11.091%
25	0.7932×10^{-2}	0.915×10^{-2}	(+) 15.287%
40	0.7928×10^{-2}	0.994×10^{-2}	(+) 25.386%

Electric-Field Measurement and Comparison

The experimental measurements of the electric-field pattern for the RF-stimulated tests were performed at two frequencies, 710 MHz, and 726 MHz. As seen in Figure 12, the patterns of both numerically simulated and experimentally measured electric fields matched each other. As mentioned, since the monopole was not calibrated, the experimentally measured electric-field measurements do not represent the actual intensity of the electric field within the cavity. The intensity of the electric field at any specific location depends on the frequency of RF waves launched. The effect of RF waves on physical properties, such as the viscosity of water, may not be linear due to having different electric field patterns at different frequencies. Hence, the change in any physical property may not be linearly correlated with the change in frequency.





Seepage Flow Numerical Simulation

The unstimulated seepage-flow model was developed based on the hydraulic conductivity value of the unstimulated test performed in the lab. The model in MATLAB interface was used to compute the spatial variations of the hydraulic head within the soil. Figure 13 shows the contour maps of the hydraulic head on fifteen vertical slices within

the sandy sample obtained using the forward model for the unstimulated test. The hydraulic head decreased gradually and uniformly from the bottom (inlet) to the top (outlet), indicating the existence of a uniform gradient along the length of the soil specimen and an upward uniform flow within the homogeneous sand sample.

The experimentally measured flow discharge in the natural sand sample during unstimulated tests was $9.34 \times 10^{-6} \text{ m}^3/\text{s}$. Additionally, the finite- difference forward model computed the flow discharge to be $9.23 \times 10^{-6} \text{ m}^3/\text{s}$. There is a small discrepancy of 1.18% between the experimental and numerical values, and the difference is due to the approximation of the cylindrical walls of the permeameter using a stepwise rectangular cubical wall.

To better understand the RF stimulation effect on hydraulic conductivity, the increase in hydraulic conductivity due to RF waves was correlated with the RF-power level. The RF-power density at each node was obtained from the RF forward model generated using COMSOL Multiphysics. Table 5 shows the experimental flow discharge, numerically computed flow discharge, and slope (β) at a frequency of 726 MHz and RF-power levels of 10, 25, and 40 Watts.

Table 5 Experimentally Measured and Numerically Computed Flow Discharge in the Natural Sand Sample at Various RF-Power Levels

RF Input Power (Watts)	$Q_{exp,st}$ (m ³ /s) (Experimental)	Slope (β) (Numerical Stimulation)	$Q_{sim,st}$ (m ³ /s) (Numerical value based on optimized (k'))	Cost Function $\frac{(Q_{exp,st} - Q_{sim,st})}{Q_{exp,st}} \times 100\%$
0	9.34110 ⁻⁶	None	9.23110 ⁻⁶	1.18%
10	10.39110 ⁻⁶	3.65110 ⁻⁸	10.11110 ⁻⁶	2.77%
25	10.78110 ⁻⁶	3.25110 ⁻⁸	10.52110 ⁻⁶	2.47%
40	11.71110 ⁻⁶	3.25110 ⁻⁸	11.42110 ⁻⁶	2.54%

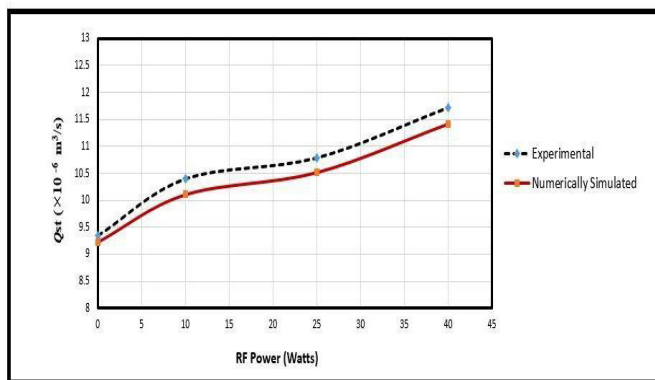
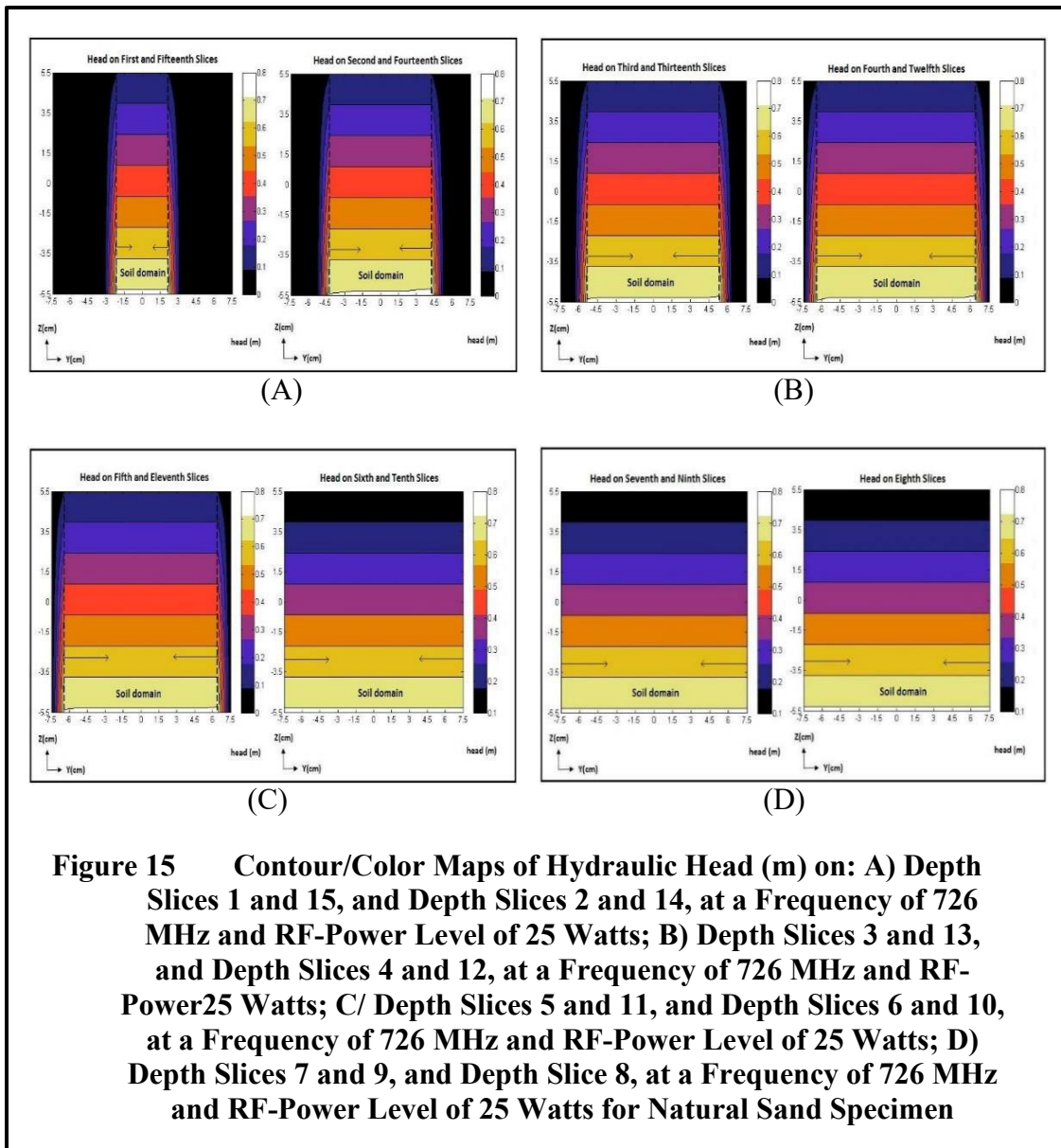


Figure 14 RF-Stimulation Flow Rate v. RF-Power for Natural Sand Specimen

Similarly, the experimentally measured and numerically computed flow discharge with respect to the RF-power levels were plotted in Figure 14. Using the optimization scheme, the cost function was minimized to less than 3%, indicating the numerically computed values reasonably matched the experimental values. In addition, the β -value at all three power levels was nearly constant.

As the optimization was completed, the optimized flow discharge, optimized hydraulic conductivity, and optimized hydraulic heads were obtained. Figure 15 displays the contour/color maps of the hydraulic heads obtained from the inverse model at a frequency of 726 MHz and an RF-power level of 25 Watts. Similar to the unstimulated case, the contour/color maps show a uniform decrease in the hydraulic head from the bottom (inlet) to the top (outlet), indicating an upward flow. There was a spatially variable alteration in the hydraulic conductivity in the X, Y, and Z directions, which is a function of the spatially variable electric-field power density. This resulted in a change in the hydraulic head within the soil specimen due to the RF-waves application, which is uniform along the X and Y directions and only varies along the Z direction. However,

change is uniform and does not manifest as a distortion in the contour/color maps of the hydraulic head.



As mentioned, the value of hydraulic conductivity and flow discharge changed due to RF stimulation. The model assumed that the scalar value of the RF power governs the alteration in the hydraulic conductivity. Hence, the variation will be the same for all components of the hydraulic conductivity tensor (i.e., the same slope, β , in all directions).

Figure 16 shows the contour/color map for k' (Z-component of the RF-stimulated

hydraulic conductivity) computed using the inverse model on Slice 7 at a frequency of 726 MHz and RF- power level of 25 Watts. Other components on the k' tensor can also be plotted. However, the hydraulic conductivity of the soil was assumed isotropic, and β was assumed the same in all directions. Therefore, k' will be isotropic. Figure 17 shows the contour/color map of the RF-power density at a frequency of 726 MHz and RF-power level of 25 Watts on Slice 7. The RF-power density at each node was obtained from the RF forward model generated using COMSOL Multiphysics.

As seen in Figure 15, the hydraulic conductivity along the Z-direction changed due to the application of RF waves. Additionally, the contour plot of the hydraulic conductivity corresponds to the variation in the power densities due to the linear

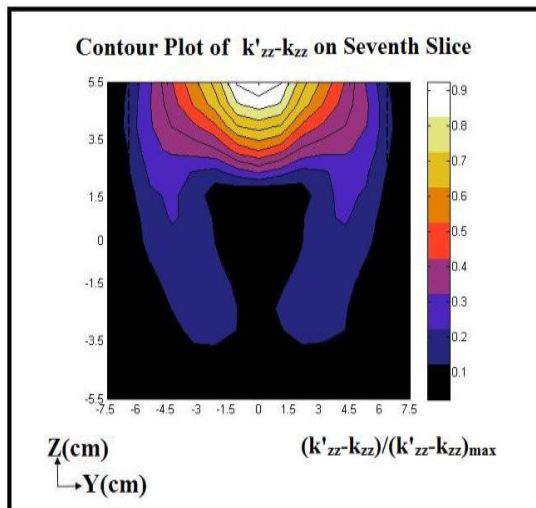


Figure 16 Contour/Color Map of Normalized Difference Between RF-Stimulated Hydraulic Conductivity Computed and Unstimulated Hydraulic Conductivity for Natural Sand Specimen Along the Vertical (Z) Direction on Slice 7

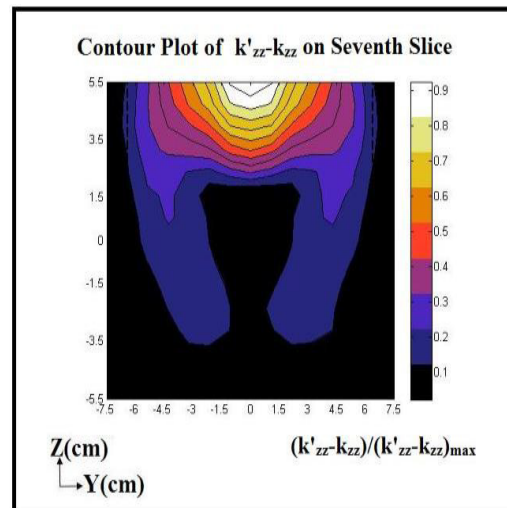


Figure 17 Contour/Color Map of Normalized Power Density for Natural Sand Specimen Along the Vertical (Z) Direction on Slice 7

relationship between the power densities at each node and RF- stimulated hydraulic conductivity.

Conclusion and Recommendations

The work outlined in this chapter demonstrates the changes in the hydraulic conductivity of glass beads and a natural sand sample due to RF waves of various frequencies.

The electric field inside the cavity was measured at various resonant frequencies and then validated against the numerically simulated electric field using COMSOL Multiphysics. The measured and numerically simulated electric fields reasonably agreed.

At all RF-power levels, for both the glass beads and natural sand, RF waves increased the hydraulic conductivity. The increase in the hydraulic conductivity was gradual with time. Additionally, for both glass-bead and natural sand samples, RF-simulated hydraulic conductivity increased with increasing RF- power levels, However, this percentage increase was observed more in the natural sand sample than the glass-bead. This could be due to the influence of the silt content within the natural sand. When RF stimulation was terminated, the hydraulic conductivity initially stabilized at its peak value. However, as time increased after termination, hydraulic conductivity slightly decreased and stabilized at a smaller value but still larger than the initial unstimulated value. The tests were not continued long enough to observe any further decrease.

The measured hydraulic conductivity was then correlated to a numerically simulated hydraulic conductivity using MATLAB interface. Results from the numerical model for the seepage flow showed a uniform decrease of the hydraulic head from the bottom (flow inlet) to the top (flow outlet) due to upward seepage flow through the

sample. In the case of RF-stimulated tests, hydraulic heads were computed using an inverse model based on an optimization scheme. After optimization, the optimized RF-stimulated numerically computed hydraulic conductivity showed a similar spatially variable pattern to that of the RF-power density.

References

- ASTM. (2006). "Standard test method for permeability of granular soils (constant head)." D2434, Philadelphia.
- Azad, S., Farid, A., and Browning, J. 2015. "Consequence of EM stimulation on Hydraulic Conductivity of a Bentonite Clayey Sample." *Environmental Geotechnics Journal*, 2 (4), 211-223, August, DOI: <http://dx.doi.org/10.1680/>.
- Azad, S; Najafi, A.; Farid, A.; Browning, J.; Barney Smith, E. 2014. "Study of Mechanisms Governing Electromagnetic Alteration of Hydraulic Conductivity of Soils." In *Geotechnical Special Publication*, 1693–1702. American Society of Civil Engineers (ASCE). doi:10.1061/9780784413272.166.
- Azad, S. 2013. "ELECTROMAGNETIC ALTERATION OF HYDRAULIC CONDUCTIVITY OF SOILS." Boise State University.
- Cole, G. L., Rajesh P.D., and Fred M.T. 2012. "Building Pounding Damage Observed in the 2011 Christchurch Earthquake." *Earthquake Engineering & Structural Dynamics* 41 (5): 893–913. doi:10.1002/eqe.1164.
- Farid, A., Najafi, A., Browning, J., and Barney Smith, E. 2019. Electromagnetic Waves' Effect on Airflow during Air Sparging. *Elsevier Journal of Contaminant Hydrology*, 220, 49-58, DOI: <https://doi.org/10.1016/j.jconhyd.2018.11.004>.
- Fetter, C.W. 2001. *Applied Hydrogeology*. 4th ed. Pearson.

- Ganainy, Hesham El, Tarek Abdoun, and Ricardo Dobry. 2012. "Centrifuge Study of the Effect of Permeability and Other Soil Properties on the Liquefaction and Lateral Spreading of Dense Sand." In GeoCongress.
- Hazirbaba, K. and Rathje. E.M. 2009. "Pore Pressure Generation of Silty Sands due to Induced Cyclic Shear Strains." *Journal of Geotechnical and Geoenvironmental Engineering*. doi:10.1061/ASCE GT.1943-5606.0000147.
- Hubbert, M. 1957. "Darcy's law and the field equations of the flow of underground fluids." *International Association of Scientific Hydrology. Bulletin*. doi:10.1080/02626665709493062.
- Ikezoe, Y., Hirota, N., Nakagawa, J., Kitazawa, K. 1998. "Making Water Levitate." *Nature* 393 (6687): 749. doi:10.1038/31619.
- Kramer, S. L. 1996. *Geotechnical Earthquake Engineering*. Pearson, 2013.
- Kuerbis, R., and Y.P. Vaid. "Sand Sample Preparation—the Slurry Deposition Method." *Soils and Foundations*, vol. 28, no. 4, Dec. 1988, pp. 107–118, https://doi.org/10.3208/sandf1972.28.4_107.
- Martin, J. R., Olgun, C.G., Mitchell, J.K., and Durgunoglu, H.T. 2004. "High-Modulus Columns for Liquefaction Mitigation." *Journal of Geotechnical and Geoenvironmental Engineering*. doi:10.1061/(ASCE)1090-0241(2004)130:6(561).
- Najafi, Atena. 2014. "THE EFFECT OF ELECTROMAGNETIC WAVES ON AIRFLOW DURING AIR SPARGING." Boise State University.
- Nakagawa, K., Soga, K., and Mitchell, J.K. "Observation of Biot compressional wave of the second kind in granular soils" (1997). *Géotechnique*, 47(1), 133-147.

- Santamarina, J. Carlos, et al. "Electromagnetism." *Soils and Waves*, John Wiley & Sons, Chichester, 2001, pp. 303–327.
- Sharp, M. K., Dobry, R., and Abdoun, T. 2004. "Liquefaction Centrifuge Modeling of Sands of Different Permeability." *Journal of Geotechnical and Geoenvironmental Engineering*. doi:10.1061/ASCE1090-0241(2003)129:121083.
- Sun, Wei, et al. "Effects of Dipole Polarization of Water Molecules on Ice Formation Under an Electrostatic Field." *ScienceDirect*, 17 Nov. 2007.

CHAPTER THREE: HYDRAULIC CONDUCTIVITY'S IMPACT ON RISE OF
EXCESS PORE- WATER PRESSURE DURING SEISMIC-INDUCED
LIQUEFACTION

Abstract

Liquefaction is a geohazard causing loss of lives and infrastructure around the world. Liquefaction results from a sudden increase in excess pore-water pressure (EPWP) in loose, saturated noncohesive, fine soils during seismic shaking. Due to the small pores and low hydraulic conductivity of these soils, the shaking- induced EPWP has less time to dissipate, leading to the loss of effective stress and, in turn, frictional shear strength of the soil (referred to as liquefaction). If a soil's hydraulic conductivity could be increased during seismic shaking, ample time could be afforded for EPWP dissipation. A potential theory, introduced by our research team, is that electromagnetic (EM) waves can increase granular soils' hydraulic conductivity. This increase can potentially lead to liquefaction mitigation.

Initially, hydraulic conductivity measurement was performed on a liquefaction-susceptible soil using a cylindrical rigid-wall parameter as well as a rectangular box made of Plexiglas. Constant-head D2434, ASTM (2006) tests were performed to measure the hydraulic conductivity of the sample. The walls of the box are connected flexibly to enable shear deformation. In addition, the sides of the box are covered with an electrically conductive transparent film, and the medium is excited at various electromagnetic frequencies and power levels using a signal generator and amplifier to alter the hydraulic conductivity of the soil.

Seismic accelerations were also induced using a shake table with the same specimen. This was repeated while the specimen was excited using EM waves of various frequencies and power levels. Thus, the relation among seismic shaking, hydraulic conductivity, and generation and dissipation of EPWP were evaluated.

Introduction

Liquefaction, a geohazard of significant concern, has proven to be a destructive force, resulting in the loss of lives and infrastructure on a global scale. This phenomenon has been observed in numerous earthquakes such as in 2011 Christchurch, New Zealand (Curbinovski, 2013), 2018 Palu, Sulawesi Island, Indonesia (Tehusijarana, 2018), and 1985 Mexico City, Mexico (Wei-Haas, 2017). Liquefaction is defined by a loss of shear strength in a soil structure due to a sudden increase in excess pore-water pressure (EPWP) from the presence of a rapid dynamic load (e.g., earthquake).

Research on soils susceptible to liquefaction—such as loosely packed, fine, water-saturated sands—demonstrated that liquefaction depends on several governing factors such as earthquake intensity and duration, groundwater depth, soil characteristics (e.g., plasticity, particle shape, i.e., rounded versus angular), placement conditions, drainage conditions, historical conditions (e.g., older soils that have previously subjected to cyclic shearing), and if a building load is present (Bolt, 1993). However, all these parameters are interconnected with the rate at which water dissipates. When water does not have enough time to dissipate during a dynamic load, a net increase in the pore-water pressure (PWP) is observed—also, referred to as EPWP (Ueng et al., 2017)—, and the effective stress ($\sigma' = \sigma - u$, kPa) approaches zero. In here, σ is total stress, σ' is effective stress, and u is PWP. A potential theory, introduced by our previous research team, is that electromagnetic

(EM) waves can increase granular soils' hydraulic conductivity. EM waves are generated when electric and magnetic fields alternate orthogonally to each other and the direction of wave propagation (for more details, refer to Acharaya, 2017). EM waves can polarize material and impact dielectric properties, such as the dielectric properties of water. According to Sun et al. (2007), when water is under the influence of an electric field, water molecules can start to reorient and align parallel to the direction of the electric field. As reorientation occurs, the hydrogen bond potentially weakens, thus decreasing the viscosity of the molecule. A decrease in viscosity potentially results in an increase in hydraulic conductivity.

Therefore, the objective of this research is to determine the relationship between hydraulic conductivity and EPWP buildup, evaluate EM waves' impact on EPWP buildup via altering hydraulic conductivity, and evaluate the potential of EM-induced liquefaction mitigation.

Background

Understanding seismic waves and hydraulic conductivity and their effect on EPWP generation and how it leads to the liquefaction of soils requires a brief description of basic background on earthquakes, hydraulic conductivity, and liquefaction. Hydraulic conductivity's effect on the generation of EPWP and its dissipation as well as the liquefaction phenomenon are discussed in this chapter.

Seismic Waves

When an earthquake occurs, three waves are produced: primary (otherwise known as pressure, P) wave, secondary (otherwise known as shear, S) wave, and Surface waves. Only P and S waves apply to this research. P waves are the strongest and fastest waves,

created by the in-phase movement of both the soil skeleton and the pore fluid. The velocity of the P wave (V_p) can reach up to or exceeds 1,500 m/s in water (Leong and Cheng, 2016). The S wave or secondary wave is the second wave released after the rupture of a fault line occurs. The S wave involves shearing rather than compression like in a P wave. The wave moves soil particles transverse to the direction of wave propagation. Due to the shearing nature of the S wave, S waves can only travel through the soil skeleton. Most soils, if not forced to vibrate at too great an amplitude, behave in an elastic linear way (Bolt, 1993). Such linear elastic behavior obeys Hooke's Law, shown in Equation 1.

$$F = -kx, \quad (1)$$

where F is the force (N), k is the constant factor characteristic of the spring (N/m), and x is the length of the expansion of the spring (m). Similarly, during an earthquake, soils will experience proportionally greater displacement in response to a larger force. An important exception to this rule is that when seismic shaking occurs in soft soils, the displacement does not always return to its original position, resulting in densification of the soil.

Hydraulic Conductivity

Soil allows water to seep through its pores that have formed interconnected paths. The seepage flow and its velocity are measured by and depend on a parameter called hydraulic conductivity. Water flows in the opposite direction of the hydraulic gradient, i.e., from points with higher hydraulic heads to those with lower hydraulic head. The flow velocity is proportional to the total head difference and is inversely proportional to the length of the flow path. Additionally, the quantity of flow is proportional to a coefficient, k , which is dependent upon the nature of the porous medium.

$$v = -k\left(\frac{dh}{dl}\right) \quad (2)$$

Equation 2 is referred to as Darcy's law, where v = Darcy's or discharge velocity (m/s), k = hydraulic conductivity (m/s), and dh = total head difference (m), dl = flow path's length (m), and $\frac{dh}{dl}$ = is known as the hydraulic gradient. The negative sign in the equation indicates that water flows from a higher total head to a lower total head.

Flow discharge is obviously proportional to a cross-sectional area and Darcy's velocity (Fetter, 2001). Darcy experimentally found that water flowed from a higher head to a lower head,

$$Q \propto (h_2 - h_1) \text{ and } Q \propto \frac{1}{L} \quad (3)$$

$$Q = vA = -k\left(\frac{dh}{dl}\right)A \quad (4)$$

where, Q = discharge flow rate (m^3/s), and A = area of the flow path (m^2).

The total head is a representative of the total energy per unit weight of water at a point. Within soils, the flow velocity is small enough to neglect the velocity head. It is derived from Bernoulli's equation and written as:

$$h = h_e + h_p = z + \left(\frac{P}{\rho g}\right), \quad (5)$$

where h = total head (m), h_e = elevation head (m), h_p = pressure head (m), z = elevation with respect to any arbitrary datum (m), P = pressure (Pa), ρ = density of water (kg/m^3), and g = gravitational acceleration ($9.806 \text{ m}/\text{s}^2$ at the sea level). The total head of water within soil can be simplified as the sum of the elevation and pressure head.

As seen in Darcy's Law, flow rate and velocity are dependent on hydraulic conductivity and connect the premise that the dissipation of EPWP generated via seismic shaking will be faster in soils with a higher hydraulic conductivity.

However, Darcy's Law is only applicable to fluids that are laminar—in other words, have a low energy flow. Fluids must overcome resistance to flow due to the velocity of the fluid. As the velocity of flow increases, the moving fluid gains kinetic energy and overcomes the initial viscous forces. As a result, the flow is no longer laminar. Reynolds number is used to help determine whether or not a fluid is laminar (Hornberger, 1998). Laminar conditions prevail when the Reynolds number is less than 10 (Fetter, 2001).

$$R = \frac{\rho v D}{\mu} \quad (6)$$

Here, R = Reynolds number (dimensionless), ρ = fluid density (kg/m^3), v = Darcy's velocity or discharge velocity (m/s), D = diameter of the passageway through which the fluid moves (m), and μ = fluid's viscosity ($\text{N}\cdot\text{s/m}^2$). For most groundwater conditions, velocity is sufficiently low, and Darcy's Law is valid (Fetter, 2001).

Intrinsic Permeability

Though flow velocity is dependent on hydraulic conductivity, hydraulic conductivity is dependent on intrinsic permeability (K_i). Intrinsic permeability is a property of a porous medium regardless of fluid properties. It is a function of the size of the pore openings, the shape of the openings, and the pore diameter. Intrinsic permeability and hydraulic conductivity of a soil can be correlated given the following equation.

$$K_i = \frac{k\mu}{\rho g} = \frac{k\mu}{\gamma} = \frac{k\mu}{g} \quad (7)$$

where, K_i = intrinsic permeability, k = hydraulic conductivity (m/s), μ = absolute or dynamic viscosity (Pa-s), γ = unit weight per volume (N/m^3), and g = gravitational

acceleration (m/s^2). One Darcy is equivalent to $1 \times 10^{-8} \text{ cm}^2$. Additionally, hydraulic conductivity is proportional to particle size.

$$Q \propto d^2 \quad (8)$$

Typical values of intrinsic permeability and hydraulic conductivity of different soils are shown in Table 2.

Generally, soils with a high void ratio can have a high permeability; however, the reverse is not true. For example, in fine soils, like silt and clay, the void ratio is high, but the pores are so small that water flows through the soil with difficulty (Fetter, 2001). Hence, these soils have lower permeability, not allowing for fast dissipation of EPWP.

Constant -Head Test

The constant-head test is a common laboratory test method used to determine the hydraulic conductivity of granular soils like sands and gravel containing little to no silt. This method allows a high flow rate of water to continuously supply a constant head. To begin the test, water is allowed to flow until the sample is fully saturated and reaches a steady state. Once a steady state has been reached, the volume of water is collected over a period of time, and the rate of flow is determined.

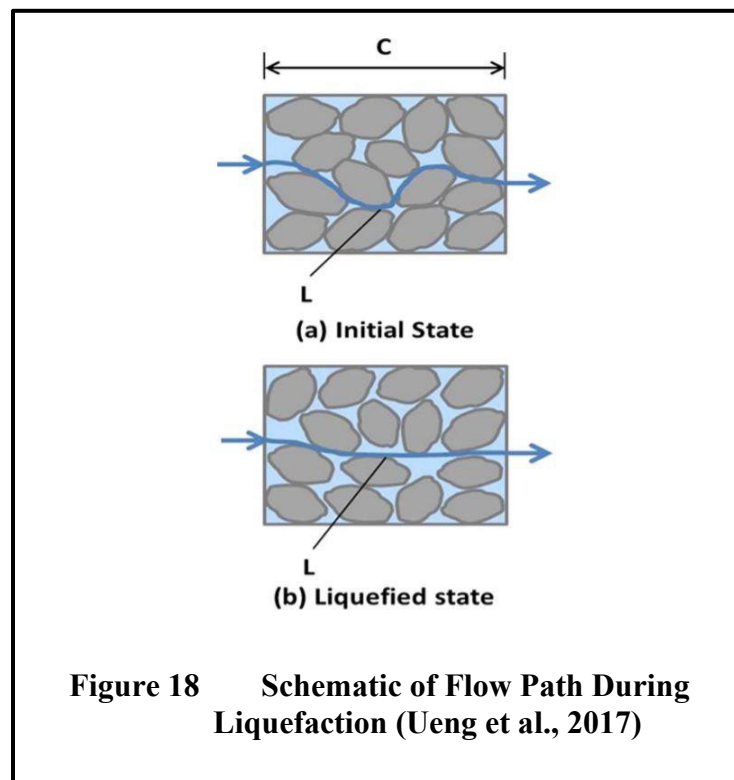
According to ASTM D2434 (ASTM, 2006), the hydraulic conductivity of a soil sample with a length L and cross-sectional area A can be computed using the following equation.

$$k = \frac{VL}{A \times \Delta h \times \Delta t} \quad (9)$$

where, V = total discharge volume (m^3), L = the length of the soil sample (m), A = cross-sectional area of the soil sample (m^2), Δh = hydraulic head loss across the soil sample (m), Δt = time interval of water collection (s).

Liquefaction

Liquefaction is a phenomenon in which the strength and stiffness of soil are reduced by a rapid dynamic load (e.g., earthquake) generating EPWP. Prior to an earthquake, the vertical total stress (σ , kPa) and effective vertical stress ($\sigma' = \sigma - u$, kPa) are both positive. In here, u is PWP. Additionally, there are contacts between soil grains. Water cannot flow as easily through these contacts, thus creating a longer flow path for water. However, during an earthquake, the soil experiences a prompt increase in the pore-water pressure (PWP, u , kPa) and soil particles lose their contacts, losing the shear strength of the soil; therefore, the effective stress approaches zero. As a result, water can more readily flow



through the soil specimen creating a shorter path for water, decreasing the time the EPWP needs to dissipate, and a net PWP is observed—also, referred to as excess pore-water

pressure (EPWP) (Ueng et al., 2017). Figure 18 illustrates this effect. According to Leong and Cheng (2016), Skempton's pore-water pressure parameter B can be used as a proxy for degree of saturation and is calculated by Equation 10.

$$B = \frac{\Delta u}{\Delta \sigma} = \frac{1}{1+n\left(\frac{K_b}{K_f}\right)} \quad (10)$$

Where Δu = change in pore-water pressure (psi); $\Delta \sigma$ = change in confining pressure (psi); n = porosity of the soil medium; K_b = bulk modulus of the soil skeleton; and K_f = bulk modulus of the fluid. The B -value increases from 0 to 1 as a dry soil reaches full saturation (if $K_b \ll K_f$). When full saturation has been reached, liquefaction has occurred.

Liquefaction Susceptibility

There are several factors that contribute to an increase in the liquefaction potential of soil. The ground motion, such as acceleration and duration, from the earthquake, determines the shear strains that cause the contraction of the soil particles and, therefore, the development of EPWP. Liquefaction potential increases as an earthquake's intensity and duration increase, e.g., earthquakes with a higher magnitude produce a larger ground acceleration as well as a longer duration of ground shaking. The shaking threshold that is needed to produce liquefaction has a maximum acceleration greater than 0.10 g or a local magnitude greater than 5.0 (Bolt, 1993).

Another factor is the location of the groundwater table. Liquefaction generally occurs near a subsurface groundwater table with unsaturated soil above the table. Only certain types of soil are subject to liquefaction. The majority of silts and clays will not liquefy during an earthquake. Uniformly graded, nonplastic soils tend to form more

unstable particle arrangements and, therefore, are more susceptible than well-graded soils. Well-graded soils can have small particles to fill in void spaces between larger particles, thus reducing the potential contraction of soil and resulting in less EPWP being generated. Soils with rounded particles tend to densify more easily than angular-shaped soil particles, making round particles more susceptible. Another characteristic to consider is confining pressure. The zone of liquefaction extends from the ground surface to a maximum depth of 15 m (50 ft). The greater the confining pressure, the less susceptible that soil is to liquefaction (Bolt, 1993).

Placement conditions are important to consider in liquefaction potential. Hydraulic fills are more susceptible to liquefaction due to the loose and segregated soil structure created by soil particles falling through the water during placement. Natural soil deposits found in lacustrine, alluvial, and marine depositional environments are, hence, all more susceptible to liquefaction (Bolt, 1993).

Soils already subjected to seismic shanking have an increase in liquefaction resistance compared to a newly formed soil structure with an identical density. Soils subjected to cyclic loading, accumulated permanent strains due to build-up of pore pressures and rearrangement of soil particles are, hence, less susceptible. Angular soil particles are more influenced by particle rearrangement during seismic shaking, but this rearrangement leads to an increase in shear strength of that soil. However, soils with rounded particles are less influenced to particle rearrangement during seismic shaking, not improving shear strength (Juneja et al., 2020). In addition, soils that have been subjected to previous cyclic loading have been shown to have a higher over-consolidation ratio (OCR) and coefficient of earth pressure at rest (k_o), and liquefaction resistance increases as

OCR and k_o increase (Bolt, 1993). After the full dissipation of EPWP, the permeability of a liquefied soil is reduced to 0.9 to 0.97 of the initial value of the soil specimen though (Ueng et al, 2017).

Current Liquefaction Mitigation Techniques

The state of practice of liquefaction mitigation, i.e., currently used in industry, includes dynamic compaction, stone columns, and compaction piles, to name a few. The goal is to increase shear strength of the soil and often referred to as ground-improvement work. These practices are utilized on already constructed sites. The State of Art, i.e., the research side of liquefaction mitigation, attempts to alter hydraulic conductivity or increase shear strength. Such practices include decreasing EPWP, microbially induced calcite precipitation (MICP), and induced partial saturation (IPS). MICP and ICS use enzymes to create cementation within liquefaction-prone soils to increase liquefaction resistance. Martin et al. (1975) demonstrated that a 1% reduction in the degree of saturation (S_r) of a saturated sand with a 40% porosity can lead to a 28% reduction in EPWP per cyclic cycle. Xia and Hu (1991) demonstrated a reduction in the degree of saturation from 100 to 97.8% led to a greater than 30% increase in liquefaction strength. Yegian et al. (2007) subjected two partially saturated samples to liquefaction both had an initial S_r of 99.5%. Electrolysis was used on one of the partially saturated samples and reduced S_r to 96.3% leading to liquefaction mitigation. The other sample was subjected to an air injection using the drainage-recharge method to mitigate liquefaction. The degree of saturation for this sample was reduced to 86%, and as a result, liquefaction was mitigated.

Electromagnetic Waves

Electromagnetic (EM) waves are generated when electric and magnetic fields alternate orthogonally to each other and the direction of wave propagation. EM waves are characterized by the intensity and frequency of waves (for a descriptive background on EM waves, refer to (Acharaya, 2017)). EM waves can polarize material and impact dielectric properties, such as in dielectric properties in water. According to Sun et al. (2007), when water is under the influence of an electric field, water molecules can start to reorient parallel to the direction of the electric field. As reorientation occurs, the hydrogen bond weakens, thus decreasing the viscosity of the molecule. Based on the literature, viscosity varies as a result of temperature according to Equation 11.

$$\mu = 0.0168 \times \rho \times T^{-0.88} \quad (11)$$

Where μ is viscosity (cP), ρ is density of water (kg/m^3), and T is temperature ($^{\circ}\text{C}$). A decrease in viscosity potentially results in an increase in hydraulic conductivity.

Methodology

Experiment Setup and Testing Procedures

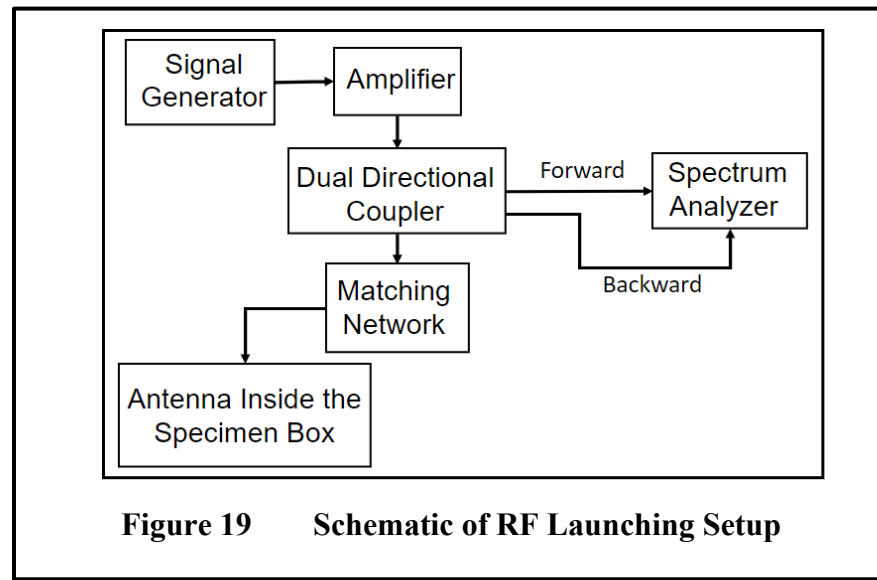
The following are the details of two series of tests. The first series evaluated the impact of RF stimulation on hydraulic conductivity of natural sand, which includes details of RF wave generation and hydraulic conductivity measurements. The second series evaluated the rise of excess pore-water pressure (EPWP) of natural sand during RF stimulation and seismic shaking. This section will also include details of earthquake emulation.

Experiment I – Simulated Hydraulic Conductivity Tests using EM Waves

To supply the power and radio frequency (RF) electric field for these tests, a magnetically coupled loop antenna was inserted into the side of the cavity perpendicular to the soil sample. The loop antenna is made of an RG-8 coaxial cable. The RF signal was generated using an Agilent Model #E440B signal generator. The frequency and amplitude are emitted into an RF amplifier to amplify the generated signal. The signal generator's amplitude should never be placed at a value greater than 0 dBm. This protects against damaging the RF amplifier. When the frequency and amplitude is set, the RF amplifier is turned on to 0 Watts or 1 mW. The conversion from dBm to Watts can be seen in Equation 12.

$$P_{(W)} = \frac{1W \times 10^{\frac{P_{(dBm)}}{10}}}{10} \quad (12)$$

To maximize power output and reduce harmful reflections back into the amplifier, the impedance of the load (setup) should be matched with that of the source (50Ω for the amplifier) using a matching network made of a series of variable capacitors. The impedance was measured using an Agilent N9320A vector network analyzer (VNA). A dual-directional coupler was also used in the network to either monitor the forward power into the device under testing (DUT) or the reflected power back into the amplifier. Figure 19 shows the schematic of the setup used for launching EM waves into the DUT.



To perform the hydraulic conductivity tests on samples to be shaken, a customized box was designed, comprised of a rigid box containing two flexible walls. The rigid box had outer dimensions of $25.4 \times 25.4 \text{ cm} \times 25.4 \text{ cm}$ ($10 \text{ in.} \times 10 \text{ in.} \times 10 \text{ in.}$) with two flexible inner walls of $21.59 \text{ cm} \times 16.51 \text{ cm}$ ($8.5 \text{ in.} \times 6.5 \text{ in.}$), 8.89 cm (3.5 in.) apart. Each wall was constructed of Plexiglas. The outer walls were covered with transparent, electrically conductive films using copper tapes to provide a resonant-cavity structure. The thickness of the walls of the box is measured to be 0.64 cm (0.25 in.). The loop antenna was installed in the vertical direction on the side of the box in between the two flexible walls and in contact with the soil sample, at the bottom center. The configuration and the size of the box and installation of the antenna at the center provided maximum field at the location where a PWP transducer is installed. Figure 20 displays the schematic of the box and its dimensions.

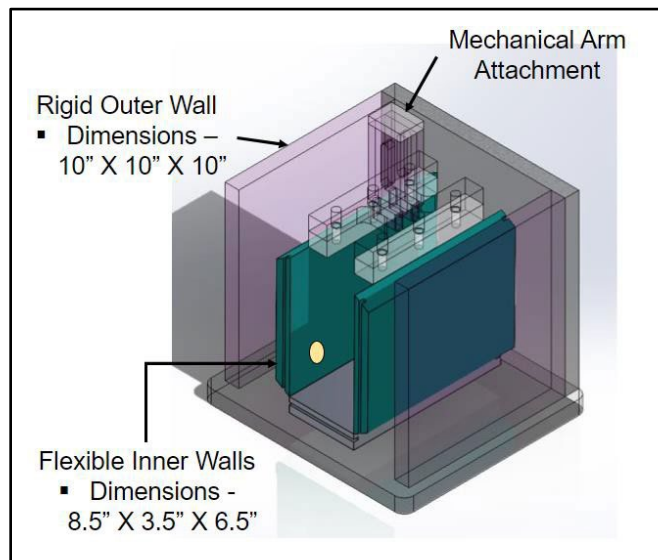


Figure 20 Schematic of Customized Box

The top of the box had a removable cover. A number of holes were drilled on the top cover forming a grid with 2 cm center-to-center spacing. During one of the electric field measurements (at RF power, $P = 40\text{W}$), a monopole probe was inserted into the soil through the drilled holes to map the electric field pattern within the cavity.

Additionally, two valves were installed at a height of 12.7 cm (5 in.) above the bottom of the box to allow drainage and recharge of water out of and into the specimen, respectively. The valve was placed on each side of the box in contact with the soil sample.

All these tests were performed on a resonant cavity filled with water and a natural sand sample. The natural sand sample was prepared using the wet-pluviation method (Kuerbis and Vaid, 1988). The natural sand was classified as poorly graded sand (SP), according to the USCS classification system. The bulk saturated density of the natural sand was measured to be 18.25 kN/m^3 . RF simulation was performed at 157 MHz and power levels of 0, 10, 20, and 40 Watts.

Experimental II – Potential Liquefaction Mitigation Tests

Seismic Shaking Setup

Seismic shaking was conducted using a one-dimensional shake table. The shake table has a tabletop dimension of 11.76 cm × 152.4 cm × 3.81 cm (44 in. × 60 in. × 1.5 in.) and has an operating shaking frequency range of 0 to 15 Hz. The nominal maximum payload mass is 1,792 kg (4,000 lbs.), and the shake table has a maximum payload horizontal eccentricity of 3 ton·m. The table can perform both the time history of earthquakes and sinusoidal shaking. For the purpose of this research, the shake table was set up to perform sinusoidal shaking.

The setup includes an accelerometer that is attached to the shake table and connects to the sensor outlet on the Dytran Model 411B1 to calculate deformation using double integration of acceleration. The Dytran is a line-operated constant-current power unit designed to integrate electrons piezo-electric (IEPE) sensors and in-line charge amplifiers. The Dytran provides 2 to 20 mA of constant current at +24 voltage dip compensator (VDC) compliance voltage. Next to the Dytran is a Groupchn PSG 9060 signal generator that has a cable running from its Channel 1 outlet to the BNC on the enclosure to start the shake table. A programmable function arbitrary wave signal generator, the PSG 9060

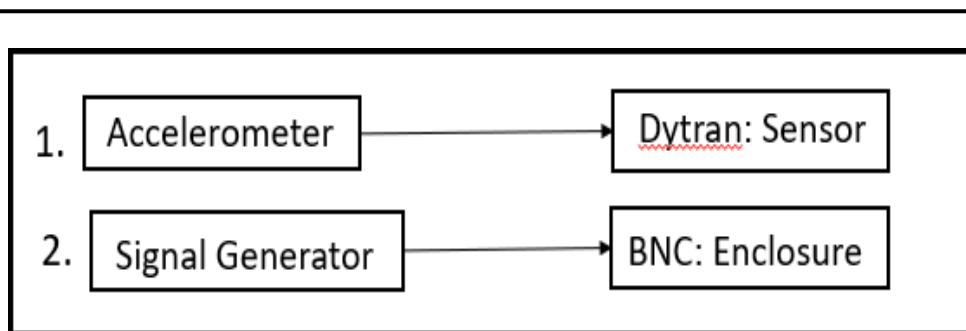


Figure 21 Schematic of Seismic Shaking Launch Setup

model, with a maximum sine-wave frequency of 60 MHz is used to generate sinusoidal shaking. The shaking frequency is set to 0 Hz and then gradually increased to 4 Hz once the shake table is turned on. The amplitude and offset are set to 0 V before the shake table is turned on. Once on, the amplitude was increased to 3 V. A schematic of the seismic shaking setup is shown in Figure 21.

Pore-Water Pressure Measurement

A pore-pressure transducer was used to measure the PWP within the soil sample before, during, and after shaking and/or RF waves were introduced into the sample. The pore-pressure measurement setup consists of a Campbell Scientific, CS-451, CR1000, data acquisition box (DAQ), and LoggerNet 4.7. CS-451 is a pore-pressure transducer that can measure pressures between 0 and 20 kPa with an accuracy of $\pm 0.1\%$. The pore-pressure transducer was placed in a customized PVC pipe fitting installed onto an outlet valve on the soil box. On the opposite end of the transducer, the wires were connected to the CR1000, data acquisition device (DAQ). Using an RS-232, the DAQ was connected to a computer via a USB. LoggerNet 4.7 was used to program the transducer to observe measurements at 1-second intervals and to record pressure every five seconds. The maximum EPWP ratio ($\Delta\mu/\sigma'$) was then calculated based on the pore-pressure data obtained using the transducer.

Results

The results from Experiments I and II are summarized in two sections. The results of Experiment I will be presented first. As mentioned, Experiment I included hydraulic conductivity tests with unstimulated and RF-stimulated tests performed on a natural sand

sample. The relationship between the effect of the RF power and hydraulic conductivity is then demonstrated.

The second section consists of the results from Experiment II—the relationship between the rise of EPWP during seismic shaking in the absence and presence of EM waves. This series of tests was also performed on samples of the same natural sand. The results were used to evaluate the shaking frequencies and acceleration at which liquefaction occurs.

Experiment I - Hydraulic Conductivity and impact of RF Waves

Constant-head hydraulic conductivity tests were performed on a natural sand sample in the absence and presence of RF waves of varying input powers and frequencies.

The results from the constant-head hydraulic conductivity test performed at zero (0) Watts are displayed in Figure 22. The test created the baseline of hydraulic conductivity for the following three tests. Hydraulic conductivity measurements took approximately 60 minutes to stabilize after flow through the sample was initiated. The hydraulic conductivity stabilized at 0.0097 cm/s (0.0038 in./s) for this natural sand sample. For better visualization of the change in the hydraulic conductivity, all measurements for each case are normalized to their respective initial unstimulated value. Figure 24 displays the fluctuations of the all the values of hydraulic conductivity measured from this experiment. The range of values fluctuated between 1.0 to 0.9975.

Figure 23 displays the results from the constant-head hydraulic conductivity test performed at 10 Watts. The amplifier was set at zero (0) Watts at the start of the experiment for an RF frequency of 159 MHz. Once the experiment was initiated, hydraulic conductivity stabilized at 0.0099 cm/s (0.0039 in./s) after 75 minutes. These values were

also normalized to their own maximum of 0.0099 cm/s (0.0039 in./s). After 75 minutes, the RF amplifier was set to 10 Watts, and measurements were recorded. The experiment ran for an hour before turning the RF amplifier back to zero (0) Watts and placing the RF amplifier on standby. No considerable change in hydraulic conductivity was observed at 10 Watts. The maximum normalized value was 0.980, showing a small reduction of 2%, considered negligible relative to variations in measurements.

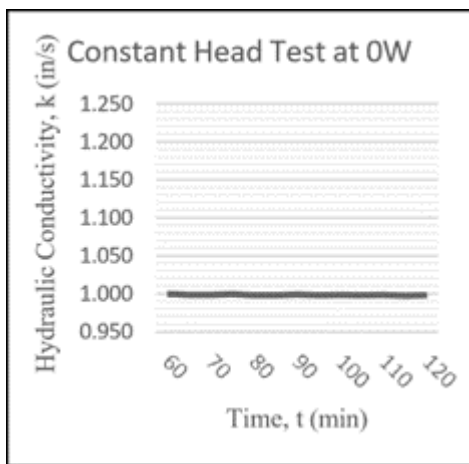


Figure 22 Constant Head Hydraulic Conductivity Test Performed at 0 Watts

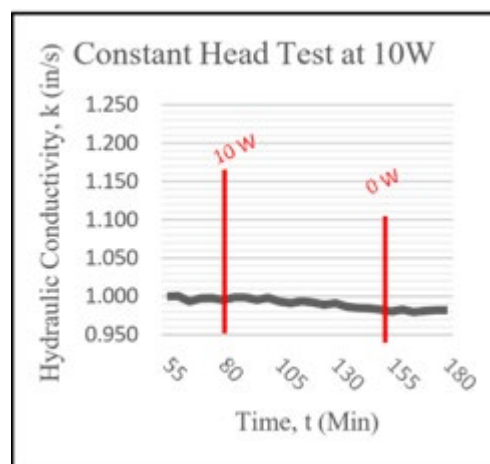
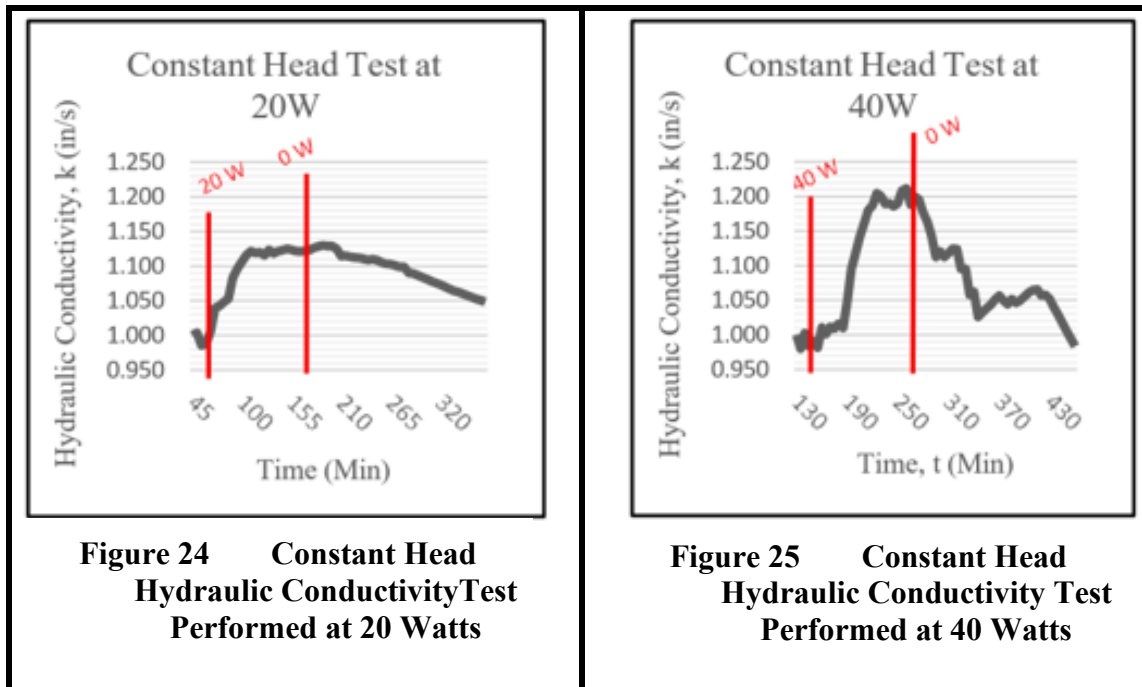


Figure 23 Constant Head Hydraulic Conductivity Test Performed at 10 Watts

The results for the constant-head hydraulic conductivity test performed at 20 Watts are displayed in Figure 24. The RF amplifier was set to zero (0) Watts prior to the start of the experiment. Once the experiment commenced, hydraulic conductivity stabilized at 0.0097 cm/s (0.0038 in/s) after 65 minutes. The results are normalized to this initial unstimulated value of 0.0097 cm/s (0.0038 in./s). At 65 minutes, the RF amplifier was set to 20 Watts and a frequency of 159 MHz, and measurements were recorded. The normalized value of hydraulic conductivity reached a peak of 1.125, or 0.0109 cm/s (0.0043 in./s), eighty minutes later, and the RF amplifier was then turned back to zero (0) Watts and placed on standby. However, the normalized value of hydraulic conductivity continued to increase to 1.130 at a time of 190 minutes. The slope of the rate of increase in the normalized value is 0.001 1/min and the hydraulic conductivity increased by 13%. The hydraulic conductivity of 0.0109 cm/s (0.0043 in./s) stayed consistent for a total of 100 minutes before the start of the decline. The variation of the peak normalized hydraulic conductivity ranges between 1.116 and 1.130, i.e., 11.6-13% increase. The slope of the decline of the normalized value was -0.0005 1/min for 180 minutes. Due to time restraints caused by clogging at the outlet, this specific experiment was concluded at a normalized value of 1.049 or 0.102 cm/s (0.004 in./s), and the experiment did not continue to hydraulic conductivity's initial value. However, the rebound slope was linear, consistent with that reported by Acharaya (2017).



A new natural sand sample was prepared for the constant-head hydraulic conductivity tests to be performed at 40 Watts due to a small amount of sand clogging the outlet valve. A geotextile staple fiber cloth (AASHTO Class 3, Sample #1A) was placed over both inlet and outlet valves and glued to the box. Once the sample was prepared, the experiment commenced with the amplifier set at zero (0) Watts. The results are displayed in Figure 25. The initial hydraulic conductivity stabilized after 130 minutes at a value of 0.0086 cm/s (0.0034 in./s). All measurements are shown as normalized to this initial unstimulated value. At 130 minutes, the RF amplifier was set to 40 Watts at a frequency of 159 MHz. After 70 minutes, the hydraulic conductivity reached a peak value of 0.0104 cm/s (0.0041 in./s), a normalized value of 1.205, i.e., showing a 20.5% increase. At 244 minutes, the RF amplifier was set back to zero (0) Watts and placed on standby. The normalized value of hydraulic conductivity continued to stay at 1.211 (i.e., showing a 21.1% increase) at 300 minutes. The slope of the rate of increase is 0.002 1/min, and the increase in the hydraulic conductivity was maintained at 21%. The hydraulic conductivity

of 0.0104 cm/s (0.0041 in./s) stayed consistent for a total of 50 minutes before the start of the decline. The variation of the peak normalized hydraulic conductivity ranged between 1.186 and 1.211 (i.e., an increase of 18.6- 21.1%). The slope of decline was -0.0011 1/min for 200 minutes.

The initial hydraulic conductivity and peak normalized hydraulic conductivity values, as well as the slope and percentage of increase in hydraulic conductivity, are shown in Table 6. It can be observed that starting at 20 Watts, there was an increase in hydraulic conductivity of 13%. Furthermore, at 40 Watts a 21% increase in hydraulic conductivity from its initial value was observed. This observation displays a linear relationship between RF-power level and hydraulic conductivity—an increase in RF-power is proportional to the increase of hydraulic conductivity. In addition, the slope of increase in hydraulic conductivity is greater at a higher RF-power, yet the slope of decrease in hydraulic conductivity to return to its initial value is also greater at a higher RF-power. The higher slope of increase at higher RF power can be attributed to the greater weakening of hydrogen bonds, which would allow for a quicker increase in viscosity and hydraulic conductivity. The slope of the rebound to the initial value is also higher (i.e., faster rebound) for higher RF powers. This behavior can be explained by considering hydrogens bonds similar to springs, where greater stretching leads to a quicker rebound after the removal of an applied force, in accordance with the principles of Hooke's Law.

Table 6 Summary of Results from Constant Head Hydraulic Conductivity Tests

Power (W)	Time for K to stabilize (min)	Initial Actual K value (cm/s)	Time Power was turned on (min.)	Peak Normalized K value	Normalized Slope (1/min)	Percentage Increase (%)	Time length of Peak K (min.)	Time Length to initial K (min.)	Normalized Slope of decrease (1/min)
00	120	0.0097	--	--	--	--	--	--	--
10	75	0.0099	75	1.00	0.000	0.00	0	0.0	0.0
20	65	0.0097	65	1.13	0.001	13.00	100	180*	0.0005
40	155	0.0086	155	1.21	0.002	21.00	50	200	0.0011

Experiment II – Potential Liquefaction Mitigation

Seismic-induced shaking tests were performed on samples of the same natural sand at varying RF input powers and frequencies. Each sample is prepared using the wet-pluviation to create very loose saturated samples. Each test involved three to four successive rounds of consequent shaking to assess pore-water pressure and settlement for samples that are consequently densified by each shaking. Additionally, a seismic-induced shaking test was performed without the presence of RF waves. The shaking table signal generator was set to output a sinusoidal wave of 4 Hz at 3 V for each test. Additionally, liquefaction was calculated by $B = \Delta u / \sigma'$, where Δu is the change in the EPWP, and σ' is the initial effective stress. During seismic shaking, EPWP increases, and when $\Delta u / \sigma'$ reaches a value of one (1), liquefaction occurs. After each test, the natural sand sample was

replaced with a new one. As mentioned, each sample is prepared using the wet-pluviation to create very loose saturated samples.

The results from the seismic-induced shaking test performed at zero (0) Watts are displayed in Figure 26. The test created the baseline for the measurement of the pore-water pressure and its rise during seismic shaking for the following three tests. As mentioned, samples are shaken until they liquefy and densify, then they are shaken again, and this is repeated consequently four times. It was expected that liquefied samples would densify and liquefy less and less. This is expected to be more pronounced from the first to the second consequently shaking due to higher potential for liquefaction for very loose samples. Hence, in total, the test at zero (0) Watts of RF power, each, includes four (4) consequent rounds of shaking. During the first round, the PWP rose and reached a peak of 0.676 kPa (0.098 psi) in 0.33 minutes, corresponding to $\Delta\mu/\sigma'$ calculated to be 0.72 at 3.18cm (1.25 in.) of settlement. For the second consequent shaking, the PWP rose and reached a peak of 0.517 kPa (0.075 psi) in 0.35 minutes with a $\Delta\mu/\sigma'$ to be found to be 0.41 at 0.64 cm (0.25 in.) of settlement. During the third consequent shaking, the PWP rose to a peak of 0.483 kPa (0.070 psi) in 1.93 minutes with $\Delta\mu/\sigma'$ equaling 0.24 where the soil settled 0.318 cm (0.125 in.). Last, during the final (fourth) consequent shaking, PWP rose to a peak of 0.614 kPa (0.089 psi) in 2.05 minutes where $\Delta\mu/\sigma'$ equaled 0.46 and no settlement occurred. The reason this was performed was to provide four samples with various densities for each RF power test. If densification is not pronounced, this would provide four results and a mean and error bar.

Figure 27 displays the seismic-induced shaking test performed at 10 Watts. The RF amplifier was set to 10 Watts and a frequency of 157 MHz before the seismic-induced shaking commenced. It was then left for 75 minutes, which corresponds to the duration required for hydraulic conductivity to stabilize during the constant-head test at 10 Watts of RF power. During the initial round of shaking, PWP reached a peak of 0.710 kPa (0.103 psi) in 0.43 minutes with $\Delta\mu/\sigma'$ equaling 1.11, which means liquefaction has occurred. Additionally, the soil sample settled 2.85 cm (1.125 in.). During the second consequent shaking of the densified sample, PWP rose to a peak of 0.469 kPa (0.068 psi) in 7.6 minutes and $\Delta\mu/\sigma'$ equaled 0.19. The soil sample settled 0.318 cm (0.125 in.). Furthermore, during the third round, PWP reached a peak of 0.490 kPa (0.71 psi) in 15.57 minutes. $\Delta\mu/\sigma'$ was calculated to be 0.19 and no settlement occurred.

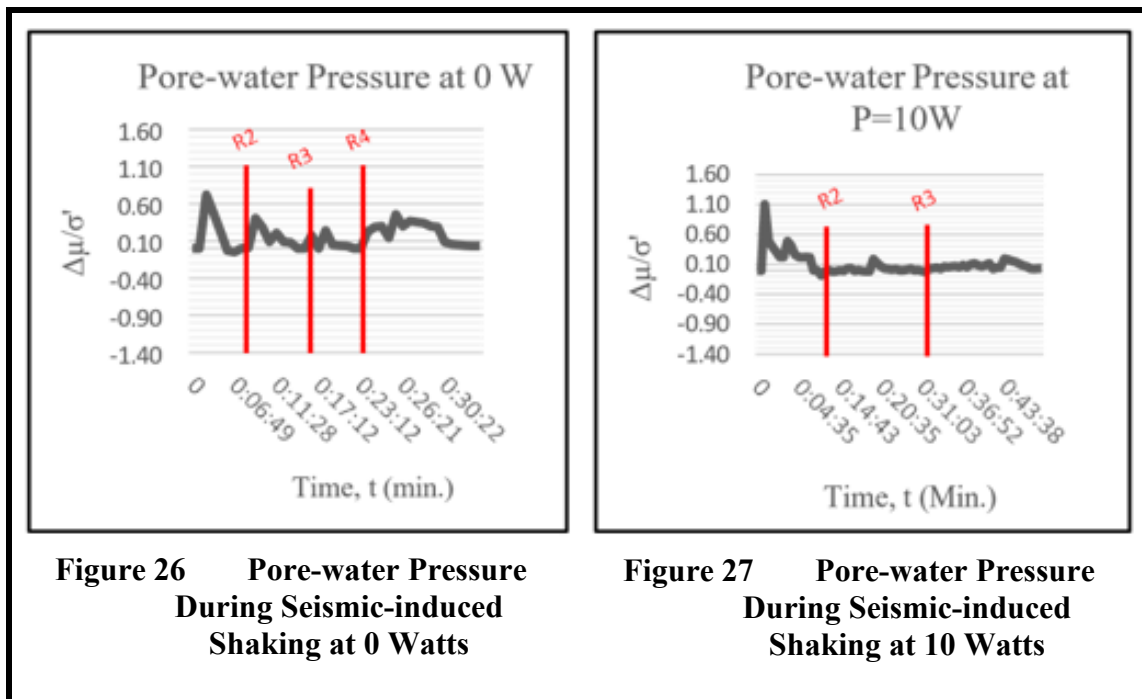


Figure 26 Pore-water Pressure During Seismic-induced Shaking at 0 Watts

Figure 27 Pore-water Pressure During Seismic-induced Shaking at 10 Watts

The results from the seismic-induced shaking test performed at 20 Watts are displayed in Figure 28. Before seismic-induced shaking commenced, the RF amplifier

was set to 20 Watts and a frequency of 157 MHz. It was then left for 145 minutes, which corresponds to the duration required for hydraulic conductivity to stabilize during the constant head test at 20 Watts. In the initial round, PWP reached a peak of 0.786 kPa (0.114 psi) in 0.5 minutes with $\Delta\mu/\sigma'$ equaling 1.57, which means liquefaction has occurred. The soil sample settled 3.175 cm (1.25 in.). During the second round, PWP rose to a peak of 0.490 kPa (0.071 psi) in 4.15 minutes. $\Delta\mu/\sigma'$ was calculated to be 0.04 and the soil settled 0.635 cm (0.25 in.). Furthermore, during the third round, PWP reached a peak of 0.710 kPa (0.103 psi) in 5.15 minutes with $\Delta\mu/\sigma'$ equaling 0.49. The soil settled another 0.318 cm (0.125 in.) Last, in the fourth round, PWP reached a peak of 0.490 kPa (0.071 psi) in 7.62 minutes. $\Delta\mu/\sigma'$ was found to be 0.1 and zero settlement occurred.

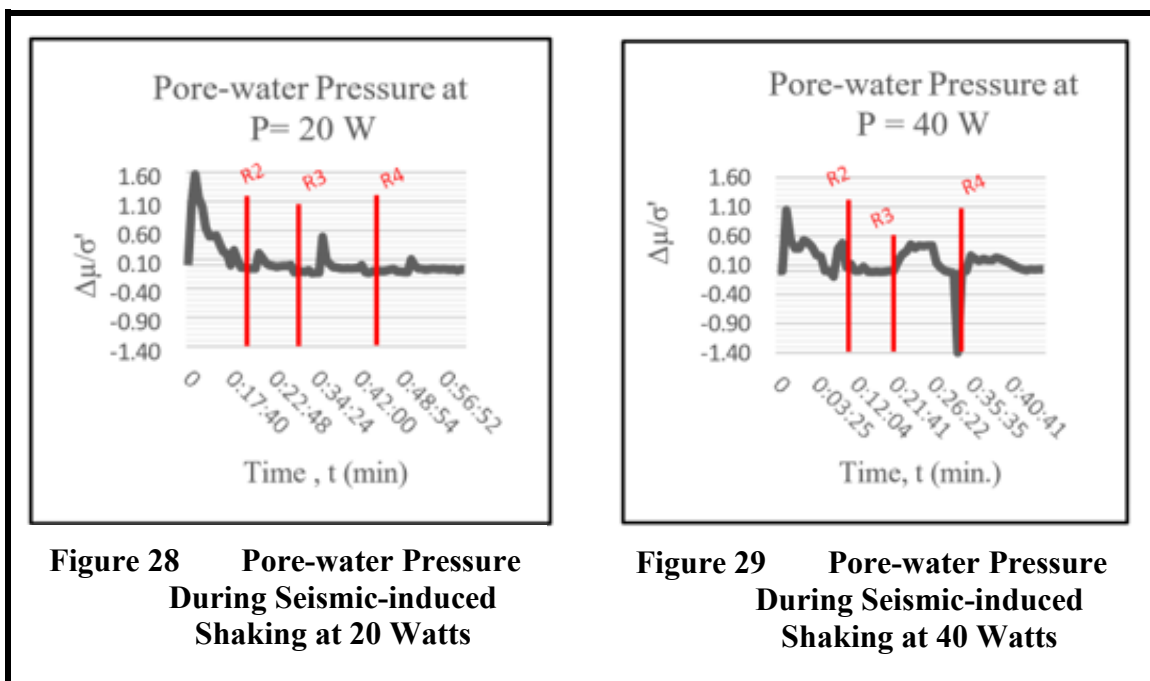


Figure 28 Pore-water Pressure During Seismic-induced Shaking at 20 Watts

Figure 29 Pore-water Pressure During Seismic-induced Shaking at 40 Watts

Figure 29 displays the seismic-induced shaking test performed at 40 Watts. The amplifier was set to 40 Watts and a frequency of 157 MHz before the seismic-induced

shaking commenced. It was then left for 166 minutes, which corresponds to the duration required for the hydraulic conductivity to stabilize during the constant head test at 40 Watts. During the initial round, PWP reached a peak of 0.696 kPa (0.101 psi) in 0.32 minutes with $\Delta\mu/\sigma'$ equaling 1.05. Liquefaction has occurred. Additionally, the soil sample settled 2.692 cm (1.06 in.) During the second round, PWP reached a peak of 0.641 kPa (0.093 psi) in 1.45 minutes and $\Delta\mu/\sigma'$ equaling 0.48. The soil sample settled 0.483 cm (0.19 in.). Furthermore, during the third round, PWP rose to a peak of 0.627 kPa (0.91 psi) in 2.32 minutes. $\Delta\mu/\sigma'$ was calculated to be 0.46 and the soil sample settled 0.318 cm (0.125 in.). Finally, in the last round, PWP reached a peak of 0.510 kPa (0.074 psi) in 3.88 minutes with $\Delta\mu/\sigma'$ equaling 0.23 and zero settlement occurred. summary of all the results from the seismic-induced shaking experiments is displayed in Table 7.

Table 7 Summary of results from seismic-induced shaking experiments

Power (Watts)	Frequency (MHz)	Experiment Number	Initial PWP (psi)	Time to Reach Peak PWP (min.)	Peak PWP (psi)	$\Delta\mu/\sigma'$	Final PWP (psi)	Settlement (in.)
0	126.034	1	0.040	0.333	0.098	0.720	0.033	1.250
		2	0.033	0.350	0.075	0.410	0.044	0.250
		3	0.044	1.933	0.070	0.240	0.048	0.125
		4	0.048	2.050	0.089	0.460	0.052	0.000
10	126.037	1	0.018	0.433	0.103	1.110	0.047	1.125
		2	0.047	7.600	0.068	0.190	0.050	0.125
		3	0.050	15.567	0.710	0.190	0.054	0.000
20	126.037	1	0.013	0.500	0.114	1.570	0.040	1.250
		2	0.040	4.150	0.071	0.040	0.066	0.250
		3	0.066	5.150	0.103	0.490	0.060	0.125
		4	0.060	7.617	0.071	0.100	0.051	0.000
40	127.037	1	0.020	0.317	0.101	1.050	0.052	1.063
		2	0.052	1.450	0.093	0.480	0.510	0.188
		3	0.051	2.317	0.091	0.460	0.050	0.125
		4	0.050	3.883	0.074	0.230	0.054	0.000

One possible improvement to this setup to allow the higher hydraulic conductivity to reflect as liquefaction mitigation is to afford water a place to which to dissipate from the sample. In other words, in the current setup, the outlet was blocked by the pore-pressure transducer. The water was filled to 15 cm (6 in.) or just above the pore-pressure transducer each time. Water also filled areas outside the two flexible walls. As the soil sample was

shaken, water would rise within the soil sample, yet not have enough space to dissipate out to the areas between the flexible walls and the side of the cavity. Even though the impact of RF waves on EPWP is observed, the setup needs to be modified such that the pore-pressure transducer would not block EPWP dissipation. In other words, as opposed to mitigating the rise of EPWP by RF waves, a faster transfer of EPWP to the pore-pressure transducer area was observed, which justifies future modifications to the experimental setup.

Additionally, the initial pore-water pressure measurement was different at the start of each experiment due to the different height of water in each setup. The height of water in the soil sample ranged from 13.97 cm to 15.56 cm (5.5 in. to 6.125 in.), demonstrating a linear relationship between the height of water and pressure. On the other hand, despite efforts to electrically isolate the pore-pressure transducer from RF waves, the transducer measurements seem to be interfered by the RF waves and are measured lower than the actual number. The amount of error produced from impact of EM waves is displayed in Table 8. Two sets of experiments were performed, where the height of water was measured at 15.24 cm and 22.86 cm (6 in. and 9 in.), respectively. Each experiment also measured PWP at RF power levels of 0, 10, 20, and 40 Watts. The initial PWP when the height of water was measured at 15.24 cm (6 in.) was 0.248 kPa (0.036 psi) at 0 Watts. According to the data in Table 8, an increase in RF power level led to a decrease in PWP. As a result, the error per 10 Watts also increased by one percent (1%). A similar linear relationship between RF power level and the percent (%) error was illustrated in the second experiment. The initial PWP when the height of water was measured at 22.86 cm (9 in.) was 1.048 kPa

(0.152 psi) at 0 Watts. When the RF power level increased, the PWP pressure decreased, resulting in the error increasing by one percent per 10 Watts of power.

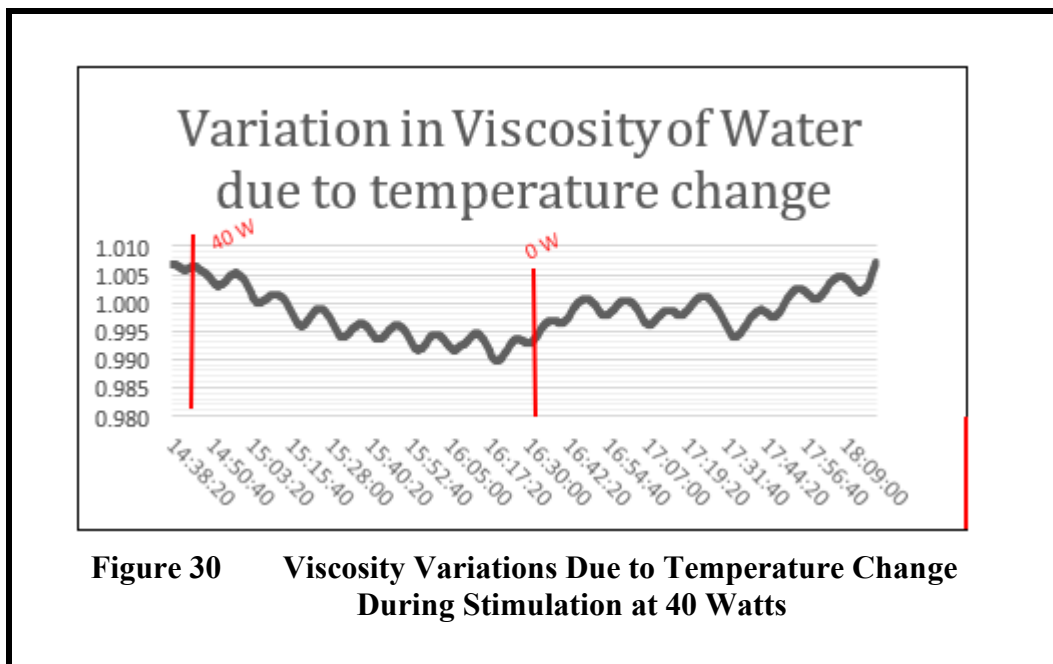
Table 8 Percentage of an Error on Pore-Water Pressure From EM Waves

H_w	Frequency (MHz)	Power (Watts)	μ_{act} (psi)	μ_{worse} (psi)	μ_{stable} (psi)	err _{worse} (%)	err _{stable} (%)
6	127.036	0	0.036	0.036	0.036	0.0	0.0
		10	0.036	0.027	0.03	-0.9	-0.6
		20	0.036	0.017	0.027	-1.9	-0.9
		40	0.036	0.013	0.019	-2.3	-1.7
9	126.233	0	0.152	0.152	0.152	0.0	0.0
		10	0.152	0.140	0.141	-1.2	-1.1
		20	0.152	0.132	0.138	-2.0	-1.4
		40	0.152	0.125	0.130	-2.7	-2.2

As mentioned, as far as the impact of EM waves on the hydraulic conductivity is concerned and above-mentioned independent of the PWP measurement, the results of a linear relationship presented from these two experiments can be attributed to that higher RF power levels induce greater weakening of hydrogen bonds among water molecules, leading to a reduction in viscosity, and in turn, increasing the hydraulic conductivity. Figure 30 displays the computed viscosity of water when power level was 40 Watts. The amplifier was set at zero (0) Watts at the start of the experiment for an RF frequency of 156 MHz. Once the experiment was initiated, the viscosity stabilized at 1.007 cP after 2 minutes. At 2 minutes, the RF amplifier was set to 40 Watts and a frequency of 156 MHz, and measurements were recorded. The value of viscosity reached a minimum of 0.990 cP around one hundred minutes later. Then the RF amplifier was

turned back to zero (0) Watts and placed on standby. The slope of decrease is -0.00017 cP/min, and the viscosity decreased by 1.7%. The viscosity of 0.99 cP stayed consistent for two minutes before it started to increase. The slope of the increase was 0.00014 cP/min for 119 minutes.

The experiment shows that the RF stimulation only increased the temperature by 0.5°C , resulting in -1.7% change in the viscosity and, in turn, 21% increase in the hydraulic conductivity. This is not consistent with the 21% increase in hydraulic conductivity. Thus, we can conclude that the RF waves' interactions with water molecules and not the direct temperature increase due to the generated heat from the RF waves causes the increase in the hydraulic conductivity.



These results correspond to Equation 11, stating that as temperature increases viscosity decreases, resulting in an inverse linear relationship. However, for this experiment, the change in viscosity due to the temperature change is negligible. A summary of these results is shown in Table 9.

Table 9 Summary of Results From Viscosity of Water Due to Temperature Change During Stimulation at 40 Watts

Power (Watts)	Frequency (MHz)	Temperature (°C)	Time to reach peak temperature (min.)	Viscosity (cP)	Slope of Change (cP/min)
0	156	24.5	2	1.007	—
40	156	24.98	100	0.990	-0.00017
0	156	24.5	119	1.007	0.00014

Furthermore, this finding about the error in the pore-pressure transducer measurement does not change the conclusions drawn from the seismic-induced shaking experiments. Removing the error would result in an even higher measured PWP under RF stimulated conditions, reinforcing the conclusion that the increased hydraulic conductivity facilitated the dissipation of EPWP toward the pore-pressure transducer. However, there is no place to afford dissipation as the pore-pressure transducer has blocked the outlet. As mentioned, a natural piezometer or better grounding of the pore-pressure transducer to minimize RF interference with the transducer need to be implemented in the future.

Conclusion and Recommendations

This research demonstrates the increase in hydraulic conductivity of natural sand due to RF waves of various power levels and explores the relationship between the rise of EPWP and seismic shaking.

Increased values of hydraulic conductivity were observed in the natural sand specimen as RF-power levels were increased. The hydraulic conductivity gradually increased with time. After turning off the power, the hydraulic conductivity showed a continued increase until it plateaued at its maximum value, followed by a subsequent decrease and return to the initial level.

During the seismic-induced shaking, liquefaction occurred at all experimented RF-power levels. A potential theory is that due to limitations of flow pathways within the cavity for water to dissipate (i.e., pore-pressure transducer has blocked the outlet) during shaking, the increased hydraulic conductivity under RF stimulation only expedited the rise of the PWP measured by the pore-pressure transducer and not mitigated liquefaction. With an increase in the RF-power level, higher value of $\Delta\mu/\sigma'$ were obtained but at a slower pace. When the RF-power level was increased further, liquefaction occurred sooner but had at a lower value of $\Delta\mu/\sigma'$. There is need for further research and modification of the setup to afford a dissipation path for water to better observe the impact of increased hydraulic conductivity—using RF waves—on liquefaction. In terms of field applications, this might mean the use of RF waves need to be mixed with other methods such as the installation of gravel-drain wells placed further apart, i.e., is the use of RF waves is mixed with installation of gravel-well drains, RF waves can help reduce the number of required wells by increasing their spacing. Research into the applications (e.g., liquefaction mitigation) of the effect of EM waves on hydraulic conductivity of soils is an ongoing and evolving field of study and requires further research.

References

- Acharya, Rakesh. "Electromagnetically Induced Alteration of Hydraulic Conductivity of Coarse-Grained Soils for Geotechnical Applications." Boise State University, 2016.
- ASTM. (2006). "Standard test method for permeability of granular soils (constant head)." D2434, Philadelphia.
- Bolt, Bruce A. "Chapter 2: Seismic Waves." Earthquakes and Geological Discovery. Scientific American Library, 1993. 26-34.
- Curbrinovski, Misko. "Liquefaction-induced Damage in the 2010-2011 Christchurch (New Zealand) Earthquakes" (2013). International Conference on Case Histories in Geotechnical Engineering. 1.
<https://scholarsmine.mst.edu/icchge/7icchge/session12/1>.
- Fetter, C.W. 2001. *Applied Hydrogeology*. 4th ed. Pearson.
- Hornberger, George M. Elements of Physical Hydrology. Edited by George M. Hornberger. 2nd ed. JHU Press. 1998.
- Juneja, Ashish, and A.K. Mohammed-Aslam. "Post-Cyclic Undrained Response of Sand and Silt." *Soil Dynamics and Earthquake Engineering* 133 (June 2020): 106138.
<https://doi.org/10.1016/j.soildyn.2020.106138>.
- Kuerbis, R., and Y.P. Vaid. "Sand Sample Preparation—the Slurry Deposition Method." *Soils and Foundations*, vol. 28, no. 4, Dec. 1988, pp. 107–118,
https://doi.org/10.3208/sandf1972.28.4_107.

Leong, E. C., and Z. Y. Cheng. "Effects of Confining Pressure and Degree of Saturation on Wave Velocities of Soils." *International Journal of Geomechanics* 16, no. 6 (December 2016). [https://doi.org/10.1061/\(ASCE\)GM.1943-5622.0000727](https://doi.org/10.1061/(ASCE)GM.1943-5622.0000727).

"Liquefaction of Soils During Earthquakes", Nov. 1985,
nehresearch.nist.gov/static/files/NSF/PB86163110.pdf.

Martin, Geoffrey R, et al. *Fundamentals of Liquefaction Under Cyclic Loading*.
Dept. of Civil Engineering, University of British Columbia, 1974.

Nakagawa, K., Soga, K., and Mitchell, J.K. "Observation of Biot compressional wave of the second kind in granular soils" (1997). *Géotechnique*, 47(1), 133-147.

Steeb, H., Kurzeja, P.S., and Schmalholz, S.M. "Wave Propagation in Unsaturated Porous Media" (2014). *Acta Mech.*, 225(8), 2435-2448.

Sun, Wei, et al. "Effects of Dipole Polarization of Water Molecules on Ice Formation Under an Electrostatic Field." *ScienceDirect*, 17 Nov. 2007.

Tehusijarana, Karina. "Central Sulawesi QUAKE, Tsunami Inflicted Us \$911 Million in Losses: Govt – Indonesia." *ReliefWeb*, The Jakarta Post, 23 Oct. 2018.
<https://reliefweb.int/report/indonesia/central-sulawesi-quake-tsunami-inflicted-us911million-losses-govt>.

Ueng, Tzou-Shin, et al. "Laboratory Tests for Permeability of Sand during Liquefaction." *Soil Dynamics and Earthquake Engineering*, vol. 100, Sept. 2017, pp. 249-56.
DOI.org (Crossref), <https://doi.org/10.1016/j.soildyn.2017.05.037>.

Wei-Haas, Maya. "How Mexico City's Unique Geology Makes Deadly Earthquakes Even Worse." *Smithsonian.com*, Smithsonian Institution, 20 Sept. 2017,

www.smithsonianmag.com/science-nature/how-mexico-citys-unique-geology-makes-earthquakes-even-worse-180964972/.

Xia, Hong, and Ting Hu. “Effects of Saturation and Back Pressure on Sand Liquefaction.” *Journal of Geotechnical Engineering*, vol. 117, no. 9, 1991, pp. 1347–1362, [https://doi.org/10.1061/\(asce\)0733-9410\(1991\)117:9\(1347\)](https://doi.org/10.1061/(asce)0733-9410(1991)117:9(1347)).

Yegian, M. K., et al. “Induced-Partial Saturation for Liquefaction Mitigation: Experimental Investigation.” *Journal of Geotechnical and Geoenvironmental Engineering*, vol. 133, no. 4, Apr. 2007, pp. 372–80. DOI.org (Crossref), [https://doi.org/10.1061/\(ASCE\)1090-0241\(2007\)133:4\(372\)](https://doi.org/10.1061/(ASCE)1090-0241(2007)133:4(372)).

Chapter Four: Conclusions

Conclusions and Recommendations

This paper encompassed two primary studies. The first study explored the impact of EM waves on the hydraulic conductivity of glass beads and a natural sand sample while validating the electric field against a numerically simulated electric field using COMSOL Multiphysics. The second study delved into the relationship between hydraulic conductivity and EM waves, as well as the relation among seismic shaking, hydraulic conductivity, and generation and dissipation of EPWP.

The first study illustrated that at all RF-power levels, for both glass beads and natural sand, RF waves increased hydraulic conductivity. A linear relationship was observed as the RF-power level increased, and the hydraulic conductivity also increased. However, the percentage of increase was observed more in the natural sand sample than in the glass bead. This could be due to the influence of silt content within the natural sand.

Subsequently, the measured hydraulic conductivity was compared to a numerically simulated hydraulic conductivity using MATLAB interface. The numerical model for seepage flow illustrated a uniform decrease of the hydraulic head from the bottom (flow inlet) to the top (flow outlet) due to upward seepage flow through the sample. For RF-stimulated tests, hydraulic heads were computed using an inverse model based on an optimization scheme. Following the optimization process, the optimized RF-stimulated numerically computed hydraulic conductivity exhibited a spatially variable pattern that closely resembled the distribution of RF-power density.

The second study demonstrated the increase in hydraulic conductivity of natural sand due to RF waves of various power levels and explored the relationship between the rise of EPWP and seismic shaking. At RF-power levels of 20 Watts and 40 Watts, RF waves increased the hydraulic conductivity of the natural sand specimen by 13% and 21%, respectively. After turning off the power, hydraulic conductivity continued to increase until it reached a maximum value, followed by a subsequent decrease to its initial value.

During seismic shaking, liquefaction occurred at RF-power levels 10, 20, and 40 Watts. A potential theory is due to the limitations of flow pathways within the cavity for water to dissipate during shaking. RF-power level 20 Watts obtained the highest value of $\Delta\mu/\sigma'$ yet took the longest amount of time to reach. RF-power level 40 Watts liquefied in the shortest amount of time but had a lower value for $\Delta\mu/\sigma'$ than 20 Watts. This requires further research and modification of the setup to afford a path for water to escape to better observe the impact of increased hydraulic conductivity—by RF waves—on liquefaction.

Future Research

Gravel drain wells present a potential solution—hydraulic conductivity in the horizontal direction drains quicker than hydraulic conductivity in the vertical direction—water would have time to dissipate, therefore, mitigating liquefaction. However, RF waves can help reduce the number of required well by increasing their spacing. Research into applications, such as liquefaction mitigation, on the effect of EM waves and hydraulic conductivity in the soil is an ongoing and evolving field of study.